

# Simulating the transport and dispersal of volcanic ash clouds with initial conditions created by a 3D plume model

Zhixuan Cao<sup>1,2</sup> Marcus Bursik<sup>3</sup> Qingyuan Yang<sup>4,5</sup> Abani Patra<sup>\*,1,6</sup>

<sup>1</sup> Mechanical and Aerospace Engineering Department, SUNY Buffalo, Buffalo, NY, USA

<sup>2</sup> Fluids Business Unit, ANSYS Inc, Lebanon, NH, USA

<sup>3</sup> Center for Geohazards Studies, SUNY Buffalo, Buffalo, NY, USA

<sup>4</sup> Earth Observatory of Singapore, Singapore, Singapore

<sup>5</sup> The Asian School of the Environment, Nanyang Technological University, Singapore, Singapore

<sup>6</sup> Data Intensive Studies Center, Tufts University, Medford, MA, USA

Correspondence\*:

Abani Patra

abani.patra@tufts.edu

## 2 ABSTRACT

3

4 Volcanic ash transport and dispersion (VATD) models simulate atmospheric transport of ash  
5 from a volcanic source represented by parametrized concentration of ash with height. Most VATD  
6 models use a source of some prescribed shape calibrated against an empirical expression for the  
7 height-mass eruption rate (MER) relation. The actual vertical ash distribution in volcanic plumes  
8 usually varies from case to case and has complex dependencies on eruption source parameters  
9 and atmospheric conditions. We present here for the first time the use of a three-dimensional  
10 (3D) plume model to represent the ash cloud source without any assumption regarding plume  
11 geometry. By eliminating assumed behavior associated with a parametrized plume geometry, the  
12 predictive skill of VATD simulations is greatly improved. To date, no VATD simulation adopts initial  
13 conditions created from first principles based on a 3D plume simulation. We use our recently  
14 developed volcanic plume model based on a 3D smoothed-particle hydrodynamic Lagrangian  
15 method, and couple the output to a standard Lagrangian VATD model. We apply the coupled  
16 model to the Pinatubo eruption in 1991 to illustrate the effectiveness of the approach. Our  
17 investigation reveals that initial particle distribution in the vertical direction, including within the  
18 umbrella cloud, has more impact on transport of ash clouds than does the horizontal distribution.  
19 Comparison with satellite data indicates that ash particles are concentrated through the depth of  
20 the volcanic umbrella cloud, and much lower than the observed maximum plume height.

21 **Keywords:** VATD, volcano, 3D plume model, initial conditions, numerical simulation, SPH, Pinatubo, ash transport, ash dispersal

## 1 INTRODUCTION

Volcanic ash, the fine-grained fraction of tephra, can be widely dispersed to synoptic and global scales, and can lead to a degradation of air quality and pose threats to aviation (Tupper et al., 2007). Identification, tracking and modeling the future movement of volcanic ash help route and schedule flights to avoid ash clouds. Numerical estimation of ash distribution using known and forecast wind fields is necessary if we are to accurately predict ash cloud propagation and spread. Numerous volcanic ash transport and dispersion (VATD) models have been developed by both civil and military aviation, and meteorological agencies, to provide forecasts of ash cloud motion (Witham et al., 2007), such as Puff (Tanaka, 1991; Searcy et al., 1998), NAME (Jones et al., 2007), HYSPLIT (Stein et al., 2015; Rolph et al., 2017) and Ash3d (Schwaiger et al., 2012). New techniques have been integrated into VATDs to satisfy increasing demands for different types of output, model accuracy and forecast reliability. This contribution explores a forward modeling method for creating initial conditions for VATD simulations, which promises to reduce the need for inversion or user intervention and improve forecasting.

Fero et al. (2009) and Stohl et al. (2011) showed that initial source conditions have significant effects on simulation of volcanic ash transport. Constantinescu et al. (2021) proved that an enhanced initial condition provides an overall better fit of the tephra deposit generated from an ash cloud than do models without a disk-like source, demonstrating the significant impact of initial condition on ash dispersion. Besides location of the eruption vent and timing of the release, traditional VATD simulation requires key global descriptors of the volcanic plume, especially plume height, grain size, eruption duration and mass loading, or alternatively, a mass eruption rate (MER). No matter how these global descriptors are obtained, they are used to furnish the initial conditions for VATDs in the form of a line-source term of a spatio-temporal distribution of particle mass. It is a common practice to pick values for these global descriptors using an empirical expression for the height-MER relation. The values for the descriptors can also be found by parameter calibration or inversion (e.g. Fero et al., 2008, 2009; Stohl et al., 2011; Zidikheri et al., 2017). One-dimensional (1D) plume models serve as an alternative option to provide these values. For example, Bursik et al. (2012) used the 1D model puffin (Bursik, 2001) to generate estimates of mass eruption rate and grain size. In some cases, an extra step is adopted to spread ash particles from the line source horizontally, resulting in an initial ash cloud in 3D space. The horizontal spreading depends on an empirical expression as well. For example, the VATD model Puff spreads particles from the line source uniformly in the horizontal direction within a given radius. Considering the complexities of volcanic eruptions, the actual ash distribution in the initial cloud should vary from case to case and with time, making it difficult to find one general expression that is suitable for all cases. It is useful therefore to investigate alternative ways for creating initial ash clouds without assumptions regarding plume geometry, or numerical inversion. This provides the major motivation of this paper.

VATD models can be categorized into Lagrangian particle tracking and Eulerian advection-diffusion types. Among several available particle tracking models, such as, Hypact (Walko et al., 1995), Puff (Searcy et al., 1998), CANERM (D'amours, 1998), and HYSPLIT (Draxler and Hess, 1998) and advection-diffusion models, such as Fall3D (Folch et al., 2009), and Ash3D (Schwaiger et al., 2012), we adopt a particle tracking model, Puff, as the primary VATD model. Puff can accept a 3D point cloud description of the starting ash cloud as an initial condition, which makes it technically easier to couple with a 3D Lagrangian plume model. Puff initializes a discrete number of tracers that represent a sample of the eruption cloud, and calculates transport, turbulent dispersion, and fallout for each representative tracer. A cylinder extending vertically from the volcano summit to a specified plume height is the standard approach to provide a simple model of the geometry of a typical ash column. Puff minimally requires horizontal wind field data. The

65 “restart” feature of Puff makes it feasible to accommodate the hand-off between a plume simulation and the  
66 Puff simulation in terms of time and length scales. We use the Hybrid Single-Particle Lagrangian Integrated  
67 Trajectory model (HYSPPLIT) (Stein et al., 2015; Rolph et al., 2017) to better understand simulation results  
68 from Puff in this study.

69 Besides parameter calibration, 1D plume models have been used to obtain global descriptors of volcanic  
70 plumes. 1D plume models (e.g. Woods, 1988; Bursik, 2001; Mastin, 2007; de’Michieli Vitturi et al., 2015;  
71 Folch et al., 2016; Pouget et al., 2016b) solve the equations of motion in 1D using simplifying assumptions,  
72 and hence depend on estimation of certain parameters, especially those related to the entrainment of air,  
73 which is evaluated based on two coefficients: a coefficient due to turbulence in the rising buoyant jet, and  
74 one due to the crosswind field. Different 1D models adopt different entrainment coefficients based on a  
75 specific formulation or calibration against well-documented case studies. The feedback from plume to  
76 atmosphere is usually ignored in 1D models. While these 1D models generate well-matched results with  
77 3D models for plumes that are dominated by wind (often called weak plumes) much greater variability  
78 is observed for strong plume scenarios (Bursik et al., 2009; Costa et al., 2016). On the other hand, 3D  
79 numerical models for volcanic plumes based on first principles and having few parametrized coefficients  
80 (Oberhuber et al., 1998; Neri et al., 2003; Suzuki et al., 2005; Cerminara et al., 2016a; Cao et al., 2018)  
81 naturally create a 3D ash cloud, which could serve directly as an initial state of the volcanic material for  
82 VATDs. However, there is no VATD simulation using such 3D ash clouds as initial conditions. In this paper,  
83 we will carry out VATD simulations using an initial state for the ash cloud based on 3D plume simulations,  
84 generated with Plume-SPH (Cao et al., 2018, 2017). The implementation techniques described in this paper  
85 can be applied to any combination of VATD model and 3D plume model even though our investigation is  
86 based on a specific VATD model and plume model.

87 The 1991 eruption of Pinatubo volcano is used as a case study. Pinatubo erupted between June 12 and 16,  
88 1991, after weeks of precursory activity. The climactic phase started on June 15 at 0441 UTC and ended  
89 around 1341 UTC (Holasek et al., 1996a). The climactic phase generated voluminous pyroclastic flows,  
90 and sent Plinian and co-ignimbrite ash and gas columns to great altitudes (Scott et al., 1996). The evolution  
91 of the Pinatubo ash and SO<sub>2</sub>louds was tracked using visible (Holasek et al., 1996a), ultraviolet (Total  
92 Ozone Mapping Spectrometer; TOMS) (Guo et al., 2004a) and infrared sensors, including the Advanced  
93 Very High-Resolution Radiometer (AVHRR) (Guo et al., 2004b). There is sufficient observational data to  
94 estimate the eruption conditions for the climactic phase of the eruption (Suzuki and Koyaguchi, 2009). The  
95 availability of calibrated eruption conditions and extensive observational data regarding ash cloud transport  
96 make the Pinatubo eruption an ideal case study.

## 2 MATERIALS AND METHODS

### 97 2.1 Plume-SPH Model

98 Plume-SPH (Cao et al., 2018) is designed to describe an injection of well mixed solid and volcanic gas  
99 from a circular vent above a flat surface into a stratified stationary atmosphere. The basic assumptions of  
100 the model are:

- 101 1. Molecular viscosity and heat conduction is neglected since turbulent energy and momentum exchange  
102 are dominant.

- 103 2. Erupted material consisting of solid with different size and mixture of gases is assumed to be well  
 104 mixed and behave like a single phase fluid (phase 2) which is valid for eruptions with fine particles and  
 105 ash.
- 106 3. Air, which is assumed to be a well mixed mixture of different gases, is assumed to be another phase  
 107 (phase 1).
- 108 4. Assume thermodynamic equilibrium and dynamic equilibrium between the two phases. As a result,  
 109 both phases share the common energy equation and momentum equations.
- 110 5. All other microphysical processes (such as the phase changes of H<sub>2</sub>O aggregation, disaggregation,  
 111 absorption of gas on the surface of solids, solution of gas into a liquid) and chemical processes are not  
 112 considered in this model.
- 113 6. The effect of wind is also not currently considered in this model.

Based on above assumptions, the governing equations of our model are given as:

$$\frac{\partial \rho}{\partial t} + \nabla \cdot (\rho \mathbf{v}) = 0 \quad (1)$$

$$\frac{\partial \rho \xi}{\partial t} + \nabla \cdot (\rho \xi \mathbf{v}) = 0 \quad (2)$$

$$\frac{\partial \rho \mathbf{v}}{\partial t} + \nabla \cdot (\rho \mathbf{v} \mathbf{v} + p \mathbf{I}) = \rho \mathbf{g} \quad (3)$$

$$\frac{\partial \rho E}{\partial t} + \nabla \cdot [(\rho E + p) \mathbf{v}] = \rho \mathbf{g} \cdot \mathbf{v} \quad (4)$$

114 where  $\rho$  is the density,  $\mathbf{v}$  is the velocity,  $\xi$  is the mass fraction of ejected material,  $\mathbf{g}$  is the gravitational  
 115 acceleration,  $\mathbf{I}$  is a unit tensor.  $E = e + K$  is the total energy which is a summation of kinetic energy  $K$   
 116 and internal energy  $e$ . An additional equation is required to close the system. In this model, the equation  
 117 for closing the system is the following equation of state (EOS).

$$p = (\gamma_m - 1) \rho e \quad (5)$$

118 where

$$\gamma_m = R_m / C_{vm} + 1 \quad (6)$$

$$R_m = \xi_g R_g + \xi_a R_a \quad (7)$$

$$C_{vm} = \xi_s C_{vs} + \xi_g C_{vg} + \xi_a C_{va} \quad (8)$$

$$\xi_a = 1 - \xi \quad (9)$$

$$\xi_g = \xi \cdot \xi_{g0} \quad (10)$$

$$\xi_s = \xi - \xi_g \quad (11)$$

124 where,  $C_v$  is the specific heat with constant volume,  $R$  is the gas constant.  $\xi$  is the mass fraction of erupted  
 125 material. The subscript  $m$  represents mixture of ejected material and air,  $s$  represents solid portion in the  
 126 ejected material,  $g$  represents gas portion in the ejected material,  $a$  represents air,  $0$  represents physical  
 127 properties of erupted material.  $\xi_{g0}$  is the mass fraction of vapor in the erupted material.

128 Three different boundary conditions are applied in this model. At the vent, temperature of erupted  
 129 material  $T$ , eruption velocity  $\mathbf{v}$ , the mass fraction of vapor in erupted material  $\xi_{g0}$  and mass discharge

rate  $\dot{M}$  are given. The pressure of erupted material  $p$  is assumed to be the same as ambient pressure for pressure-balanced eruption. The radius of the vent is determined from  $\rho$ ,  $\dot{M}$  and  $\mathbf{v}$ . Non-slip wall boundary condition is applied to the flat ground, where we enforce the velocity to be zero. With further assumption that the ground is adiabatic, internal energy flux, which consists of heat flux and energy flux carried by mass flux, vanishes on the wall boundary. Pressure outlet boundary condition is applied to the surrounding atmosphere where the pressure is given. Except for the pressure, boundary values for density, velocity, and energy are determined by numerical calculation from the conservation laws. The initial condition for Plume-SPH is created based on the atmosphere profile before the eruption.

The governing equations, EOS, boundary conditions, and initial conditions establish a complete mathematical model. The model posed over the computational domain is then discretized using smoothed particle hydrodynamics (SPH) method (Gingold and Monaghan, 1977) available in the tool Plume-SPH (Cao et al., 2017, 2018) using two types of SPH particles: 1) particles of phase 1 to represent ambient air, and 2) particles of phase 2 to represent erupted material. So before the eruption, the computational domain is fully occupied by particles of phase 1. During the eruption, particles of phase 2 are injected into the computational domain. The discretized model is then converted into a large computation task in the Plume-SPH tool based on a parallel data management framework (Cao et al., 2017).

The input parameters for Plume-SPH include the eruption condition at vent, the material properties, and a profile of the atmosphere. The eruption parameters, material properties and atmosphere for the “Strong plume–no wind” case in the recent comparison study on eruptive column models (Costa et al., 2016) are adopted. Eruption conditions and material properties are listed in Table 1. Note that the density of erupted material at the vent and radius of the vent can be computed from the given parameters. The eruption pressure is assumed to be the same as the atmospheric pressure at the vent, hence is not given in the table. The vertical profiles of atmospheric properties were based on the reanalysis data from European Centre for Medium-Range Weather Forecasts (ECMWF) for the period corresponding to the climactic phase of the Pinatubo eruption.

Running of Plume-SPH updates physical quantities, such as temperature, velocity, and the position of SPH particles in each time step. During Plume-SPH simulation, SPH particles of phase 2, which represent the erupted material, are injected from the eruption vent into the computation domain with an initial injection velocity. As they move upwards, these particles will get mixed with SPH particles of phase 1, which represent the air, during the whole simulation. Their physics quantities get updated as well. After the simulation, the computation domain will be filled with SPH particles of both phase 1 and phase 2. Removing all SPH particles of phase 1 from the computation domain, all of the remaining SPH particles represent the erupted material, which naturally forms a plume (see Fig. 1).

## 2.2 Puff and Initial Ash Cloud

Puff (Tanaka, 1991; Searcy et al., 1998) is a dynamic pollutant tracer model. The model is based on a 3D Lagrangian form of the fluid mechanics, in which the material transport is represented by the fluid motion, and diffusion is parameterized by a stochastic process of random walk. Here, the model is constructed by a sufficiently large number of Lagrangian tracer particles with a random variables  $\mathbf{R}_i(t) = (x(t), y(t), z(t))$ , where  $i = 1 \sim M$ , which represent position vectors of particles from the origin of the ash source at the time  $t$ .  $M$  is the total number of Lagrangian tracer particles, a sample of all the ash particles.

$$\mathbf{R}_i(t + \Delta t) = \mathbf{R}_i(t) + \mathbf{W}(t)\Delta t + \mathbf{Z}(t)\Delta t + \mathbf{S}_i(t)\Delta t \quad (12)$$

170 Here,  $\mathbf{W}$  accounts for local wind advection,  $\mathbf{Z}$  is generated by Gaussian random numbers and accounts  
 171 for turbulent dispersion, and  $\mathbf{S}$  is the terminal gravitational fallout velocity or settling speed, which depends  
 172 on a tracer's size.

173 A collection of tracer particles can be used to start a Puff simulation. The tracer particles have three basic  
 174 properties, age, size and position. The age of each particle is the elapsed time from when it was released.  
 175 Ash particles in the initial ash cloud have zero age. Initial ash size distribution is assumed to be log-normal.  
 176 According to a mean and standard deviation provided by the user, Puff assigns size to each particle. Puff  
 177 initializes the position of each particle according to semiempirical expressions. The height of each particle  
 178 is determined according to the specified distribution from the surface (1000 mbar  $\cong$  0 m) to the top of the  
 179 plume height,  $H_{max}$ , which is given by the user. Puff also supports reading predefined initial ash clouds  
 180 from a file, containing the coordinates of all tracer particles.

181 Vertical particle distribution in Puff is usually based on the Poisson distribution. For the Poisson  
 182 distribution, the vertical height of ash particles is given by Eq. (13):

$$H = H_{max} - 0.5H_{width}P + H_{width}R \quad (13)$$

183 where  $P$  is an integral value drawn from a Poisson distribution of unit mean,  $R$  is a uniformly distributed  
 184 random number between 0 and 1,  $H_{max}$  is the maximum plume height,  $H_{width}$  represents an approximate  
 185 vertical range over which the ash will be distributed. So for Poisson distribution, the user can specify two  
 186 parameters,  $H_{max}$  and  $H_{width}$ . Another commonly used vertical ash distribution in VATD simulation is  
 187 Suzuki. For the Suzuki plume shape (Suzuki et al., 1983), the ash mass vertical distribution is assumed to  
 188 follow the Eq. (Eq. (14)):

$$Q(z) = Q_m \frac{k^2(1 - z/H_{max})\exp(k(z/H_{max} - 1))}{H_{max} [1 - (1 + k)\exp(-k)]} \quad (14)$$

189 Where  $Q_m$  is the total mass of erupted material,  $k$  is shape factor, which is an adjustable constant that  
 190 controls ash distribution with height. A low value of  $k$  gives a roughly uniform distribution of mass with  
 191 elevation, while high values of  $k$  concentrate mass near the plume top. So for Suzuki distribution, besides  
 192 the plume height  $H_{max}$ , there is another user specified parameter,  $k$ .

193 Puff initializes the horizontal distribution of ash particles according to semiempirical expression as well.  
 194 Puff uses a uniformly distributed random process to determine ash particle locations in a circle centered  
 195 on the volcano site. The maximum radius (at plume top) at which a particle can be located is given as  
 196 "horizontal spread". The horizontal displacement from a vertical line above the volcano is a random value  
 197 within a circle of which the radius equals the "horizontal spread" multiplied by the ratio of the particle  
 198 height  $H$  to the maximum  $H_{max}$ , see Eq. 15. So the resulting shape of the particle distribution within the  
 199 plume is an inverted cone in which particles are located directly over the volcano at the lowest level and  
 200 extend out further horizontally with increasing plume height.

$$r(H) = r_{max}H/H_{max}R \quad (15)$$

201 where  $r(H)$  is the radius of the horizontal circle, within which all particles at the height of  $H$  are located.  
 202  $r_{max}$  is the horizontal spread.  $H$  is the height,  $R$  is an uniformly distributed random number between 0 and  
 203 1.

In summary, particle distributions in the initial ash cloud are controlled by several parameters, for example,  $H_{max}$ ,  $H_{width}$ , and  $r_{max}$  if the user chooses to use semiempirical expressions, Eq. (13) and (15). Users can optimize or calibrate these parameters to adjust the initial condition for Puff so that the simulated results match better with observations. Besides the initial ash cloud, other input parameters for Puff are diffusivity in the vertical and horizontal directions, start and end time of the eruption, and eruption duration. When creating initial conditions from output of Plume-SPH, the total number of Lagrangian tracers is the count of all SPH particles of phase 2 in the plume. The same total number of Lagrangian tracers are used when creating the initial ash cloud based on semiempirical expressions. All input parameters for Puff are listed in Table 2.

## 2.3 Creation of Initial Ash Cloud From Plume-SPH Output

In this study, we convert the output of Plume-SPH into initial ash cloud which serves as the initial condition for Puff. The method proposed consists in generating the initial ash cloud directly from Plume-SPH, foregoing assumptions and estimates, or inverse modeling, regarding ash injection height and timing. The steps to create an initial ash cloud based on the raw output of Plume-SPH are shown in Fig. 1. The initial ash cloud is created from SPH particles of phase 2, which represents the erupted material in the model. After reaching the maximum rise height and starting to spread horizontally, particles of phase 2 form an initial umbrella cloud (Fig. 2). The 3D plume simulation is considered complete once the umbrella cloud begins to form. Parcels that will be transported by the ambient wind are those above the “corner” region, where mean plume motion is horizontal rather than vertical. With such consideration, we introduce an elevation threshold, which is the lower elevation limit of the ash that will be transported by the VATD. All SPH particles with elevation lower than the threshold are excluded when creating the initial ash cloud. The inflection point from vertical raising to horizontal spreading happens around 15 km according to the averaged vertical velocity ((d) in Fig. 2) and horizontal velocity ((e) in Fig. 2)). Below this inflection point, particle trajectories are primarily vertical in the stalk-like eruption column. Above this level, particle trajectories are primarily horizontal, as they flow into the umbrella cloud gravity current. So we choose 15 km to be the elevation threshold in this study.

Considering that SPH particles are only discretization points, each is assigned a grain size according to a given total grain size distribution (TGSD) (Paladio-Melosantos et al., 1996), and a concentration according to the mass and volumetric eruption rate. The Plume-SPH discretization points are thus switched to Puff Lagrangian tracer particles having grain sizes and concentrations. The coordinates of these tracer particles, which are initially in the local Cartesian coordinate system of Plume-SPH, are converted into Puff’s global coordinate system, which is given in terms of (*longitude, latitude, height*). Puff takes the initial ash cloud, consisting of the collection of Lagrangian tracer particles with grain size and concentration, and propagates from time  $t$  to time  $t + \Delta t$  via solution to an advection/diffusion equation (Eq. (12)).

To summarize, there are four steps to create an initial ash cloud from the raw output of Plume-SPH:

1. filter by SPH particle type to select SPH particles that represent erupted material (phase 2)
2. filter by a mean velocity threshold to select the upper part (above the “corner” region) dominated by horizontal transport
3. switch SPH discretization points to Lagrangian tracer particles, by assigning grain size to each particle
4. convert coordinates of the SPH Lagrangian tracers into the VATDs’ geographic coordinate system

244 The features of the volcanic plume and resulting initial ash cloud used in the case study are shown in Fig. 2.  
245 It is important to point out that since both Plume-SPH and Puff are based on the Lagrangian method, there  
246 is no extra step of conversion between an Eulerian grid and Lagrangian particles.

## 247 2.4 Puff Restart

248 The plume and ash transport models are run at different time scales and length scales. The spatial and  
249 temporal resolutions of the plume simulations are much finer than those of the ash transport model. It takes  
250 tens of minutes (600 s in this case) for the Pinatubo plume to reach a steady height. However the eruption  
251 persisted for a few hours (9 hours for the climactic phase of Pinatubo eruption), and it may be necessary  
252 to track ash transport for days following an eruption. At present, it is too computationally expensive to  
253 run 3D plume simulations of several hours in real time. In order to handle the difference in time scale, we  
254 mimic a continuing eruption with intermittent pulses releasing ash particles. In particular, we restart Puff at  
255 an interval of 600 s, i.e., the physical time of the plume simulation to reach a steady height. At every Puff  
256 restart, we integrate the output of the last Puff simulation and Plume-SPH into a new ash cloud. This new  
257 ash cloud serves as a new initial condition with which to restart a Puff simulation. A sketch demonstrating  
258 the overall restart process is shown in Fig. (3). The total number of Lagrangian tracer particles used in Puff  
259 thus equals the summed number of particles in all releases. The total number of tracer particles is therefore  
260 no longer a user-selected parameter. Fero et al. (2008) proposed using more realistic time-dependent plume  
261 heights. We do not adopt that strategy here for simplicity, although the idea would be straightforward in  
262 execution, given time-dependent eruption conditions.

## 3 RESULTS

263 Transport of volcanic ash resulting from the Pinatubo eruption on June 15, 1991, is simulated using two  
264 different initial conditions. The first type of initial condition is created in a traditional way according to  
265 user specified parameters ( $H_{max}$ ,  $H_{width}$  and  $r_{max}$ ) and the semiempirical plume shape expressions ( Eq.  
266 (13) and (15)). We use the observed plume height (40 km) as  $H_{max}$  and adopt two other parameters from  
267 a previous study(Fero et al., 2008). The second type of initial condition is created by the new method  
268 proposed in this paper. To create initial conditions using the new method described in this paper, the plume  
269 rise is simulated first by Plume-SPH. Then the initial ash cloud is obtained by processing the raw output of  
270 Plume-SPH following steps described in Sec. 2.3. Except for initial conditions, the simulation parameters  
271 that control the VATD simulation are the same for both simulations. Simulated ash transport results are  
272 compared against observations.

273 The simulation results using different initial conditions are compared with TOMS SO<sub>2</sub> and AVHRR  
274 BTD (Brightness Temperature Difference) ash cloud map imagery (Fig. 4). The Puff simulation results are  
275 post-processed by the following steps to calculate the relative concentration.

- 276 1. The 3D computational domain is discretized into a collection of cells (latitude, longitude, elevation),  
277 each cell is of size 0.2 degree × 0.2 degree × 1 km
- 278 2. Find the cell that has the maximum number of particles (tracer particles); say the maximum number of  
279 particles is  $N_{max}$ .
- 280 3. Exclude all cells that have fewer than five particles.
- 281 4. Calculate the relative concentration of each cell by dividing the number of particles in the cell by  
282  $N_{max}$ .

283 In the contour, we plot the relative concentration of the cell that has maximum number of particles at a given  
 284 (*latitude, longitude*). In addition to the relative concentration, we also plot the contours of maximum  
 285 height of the ash cloud (Fig. 5), which is obtained by the following post-processing steps.

- 286 1. The 3D computational domain is discretized into a collection of cells (latitude, longitude, elevation),  
 287 each cell is of size 0.2 degree × 0.2 degree × 1 km  
 288 2. Exclude all cells that have fewer than five particles.  
 289 3. The maximum height is the cell center height of the top cell among all cells with the same  
 290 (*latitude, longitude*).

291 We also calculated the Figure of Merit in Space (FMS) according to the definition:

$$FMS = \frac{(\text{area of intersection of Puff forecast footprint and satellite image extent})}{(\text{area of union})}$$

292 The differences between simulated ash transport by the “Semiempirical initial cloud + Puff” and “Plume-  
 293 SPH+ Puff” conditions are significant. We first check the maximum relative concentration in Fig. 4. At 23  
 294 and 31 hours after the beginning of the climactic phase, the simulated ash concentration based on the initial  
 295 conditions created from Plume-SPH is visibly closer to observation than that based on the initial condition  
 296 generated from semiempirical expressions, especially in terms of the location of the highest concentration  
 297 region. This is confirmed by the FMS, which is 0.249 (23 hours) and 0.269 (31 hours) for Plume-SPH  
 298 results, and 0.063 (23 hours) and 0.065 (31 hours) for semiempirical initial clouds. Around 55 hours after  
 299 the beginning of the climactic phase, the disparity between observation and simulation becomes more  
 300 obvious. Ash in the “Semiempirical initial cloud + Puff” simulation is located far west of the observed,  
 301 with a FMS value equal to 0.058. The high concentration area of the “Plume-SPH + Puff” simulation, even  
 302 though closer to observation, has also propagated further downwind than in the observation. The FMS goes  
 303 down to 0.085.

304 While most of our work is based on the Puff VATD it is useful to compare the maximum cloud height in  
 305 Fig. 5 with the wind field indicated in the popular VATD, HYSPLIT’s forward trajectory tracking (Fig. 6).  
 306 The comparison reveals that the ash cloud is being transported in two separate, main layers (directions)  
 307 independently. From Fig. 6, we can see that the wind between elevations of 10 km and 15 km blew from  
 308 north-east to south-west, while winds of higher elevation blew from east to west. This vertical wind shear  
 309 naturally separated the ash cloud into two layers. In the “Semiempirical initial cloud + Puff” results, the  
 310 lower elevation layer is missing, which is the most important factor causing differences between these two  
 311 simulation results (Fig. 4). Even for the upper layer, the maximum cloud height of the “Semiempirical  
 312 initial cloud + Puff” simulation results is higher than that of the “Plume-SPH+ Puff” simulation. Such  
 313 differences cannot be captured by metrics based on footprint, such as FMS. At 55 hours after the eruption,  
 314 the observed high concentration ash, which is at a relatively low elevation (inferred from the wind direction  
 315 at different elevations in Fig. 6 and the eruption location), is missing in the “Plume-SPH + Puff ” simulation  
 316 results. This leads to the large decrease of FMS values from 0.269 to 0.085. One possibility is that these  
 317 ash clouds are from eruptions after the climactic phase. In our current simulation, we use the eruption  
 318 condition for the climactic phase generating plume height for the climactic phase, but satellites see ash and  
 319 SO<sub>2</sub> from all eruption phases.

320 The only difference in initial conditions between these two simulations is the distribution of ash parcels.  
 321 The main difference between simulation results from the “Plume-SPH + Puff” and the “Semiempirical

322 initial cloud + Puff" runs can thus be directly attributed to the initial ash particle distribution, which we  
323 discuss further in the following section.

324 **3.1 Effect of plume height ( $H_{max}$ )**

325 In this section, we discuss the vertical distribution of ash particles in the initial ash cloud. The majority  
326 of volcanic ash particles are usually injected at an elevation lower than the plume height. For instance,  
327 Holasek et al. (1996a,b) reported the maximum Pinatubo plume height as  $\sim 39$  km while the cloud heights  
328 were estimated at  $\sim 20$  -  $25$  km. Self et al. (1996) reported that the maximum plume height could have  
329 been  $> 35$  km, but that cloud heights were  $23$  -  $\sim 28$  km after  $\sim 15$  -  $16$  hours. The neutral buoyancy  
330 height of the Pinatubo aerosol cloud was estimated with different methods at:  $\sim 17$  -  $26$  km (lidar) by  
331 DeFoor et al. (1992),  $\sim 20$  -  $23$  km (balloon) by Deshler et al. (1992),  $\sim 17$  -  $28$  km (lidar) by Jäger (1992),  
332 and  $\sim 17$  -  $25$  km (lidar) by Avdyushin et al. (1993). Based on comparison between simulated clouds with  
333 early infrared satellite imagery, Fero et al. (2008) reported that the majority of ash was transported between  
334 16 km and 18 km. These observations make good physical sense, as particles are concentrated near the  
335 intrusion height of the umbrella cloud, not near the plume top, because the plume top is due to momentum  
336 overshoot. However, the empirical expressions for the height-MER relation, which are commonly adopted  
337 to create initial conditions for VATD simulations, tend to place the majority of ash particles closer to the  
338 top if one uses observed plume height in the empirical expressions.

339 Here we investigate two commonly used plume shapes, the Poisson (see Eq. (13)) and Suzuki (see Eq.  
340 (14)). Particle distributions (in terms of mass percentage or particle number percentage) in the vertical  
341 direction in the initial ash cloud are shown in Fig. 7. In that figure, the vertical particle distribution based  
342 on Plume-SPH output is compared with the vertical particle distribution based on semiempirical shape  
343 expressions. Both Poisson and Suzuki distributions in Fig. 7 take  $H_{max} = 40$  km, which is close to the  
344 reported observed plume height. When adopting the Poisson distribution, ((c) in Fig. 7), the majority of the  
345 particles are between  $30$  -  $\sim 40$  km. Obviously, the Poisson function distributes the majority of ash at a  
346 higher elevation than was observed (e.g. Fero et al., 2008). As for the Suzuki distribution, (d) in Fig. 7, the  
347 majority of ash particles also occur in a range that is significantly higher than 25 km. Note that in the plot  
348 (d), the Suzuki constant  $k$  is set to 4, which is commonly used for sub-plinian and plinian eruption columns  
349 (Pfeiffer et al., 2005). As for initial ash clouds in Plume-SPH simulations, most ash particles are distributed  
350 between  $\sim 17$  -  $28$  km, which matches well with observations. The plume height is also consistent with  
351 observation.

352 For the Poisson distributions, the ash particles cannot be lower without changing the plume height. To  
353 distribute the majority of ash particles at a lower elevation, the plume height must be reduced to a value  
354 smaller than the observed plume height. Adjusting parameters such as plume height in the empirical  
355 expression is actually the traditional source term calibration method. A set of initial ash clouds using  
356 different plume heights based on the Poisson distribution is shown in Fig. 8. The plume heights adopted in  
357 plume shape expressions are not obtained from any plume model or observation of plume height, but by  
358 *a posteriori* calibration to later-observed ash cloud transport heights. For Suzuki distribution, adjusting  
359 the Suzuki constant can adjust the distribution of ash particles in vertical direction. As shown in Fig. 7,  
360 when  $k$  is equal to 1 (see (e)), the majority of ash particles are at a lower elevation than observation. With  
361  $k = 3$  and  $k = 6$  (figure (g) and (h)), the majority of ash particles are at a higher elevation than observation.  
362 When  $k$  is set to 2 (see (f)), we can see that the majority of ash particles are roughly distributed in the range  
363 17 - 28 km. But the shape does not look like a typical plume, as particles are more uniformly distributed in  
364 the vertical direction. In addition, the "best fit" Suzuki constant is different from the typical value, which

365 is 4 (Pfeiffer et al., 2005), for sub-plinian and plinian eruptions, meaning that we can not apply previous  
366 experiences into the semiempirical expression for this eruption.

367 The ash clouds created by the Poisson distribution with different plume heights are used as initial  
368 conditions in Puff simulations, whose results are shown in Fig. 11. Except for the plume height, all other  
369 parameters for creating an initial ash cloud are the same as those in Table 2. Of course, the range over which  
370 the majority of ash particles is located is lower when using lower plume heights. Figure 11 thus shows that  
371 the plume height has a significant influence on the ash transport simulation. The maximum heights of the  
372 simulated ash cloud are completely different when using different  $H_{max}$  values in the Poisson expression.  
373 When the plume height is 10 km, the ash lags behind that observed and its FMS is 0.055, which is very  
374 close to FMS when  $H_{max}$  is 40 km. For the cases that  $H_{max}$  is 20 km and 30 km, the FMS values are 0.121  
375 and 0.142 respectively. Taking 20 km as the plume height better represents the lower elevation portion of  
376 the ash cloud, while taking 30 km as the plume height better represents the higher elevation portion of the  
377 ash cloud.

378 Simulation results based on a calibrated plume height of 30 km show a footprint similar to those of  
379 “Plume-SPH + Puff”, although smaller in terms of area. However, the initial ash cloud created by a Poisson  
380 distribution with a plume height around 35 km generates the best match with observation in terms of FMS  
381 metric, with the FMS value reaching 0.227. That is to say, a plume height lower than the real plume height  
382 is required by the Poisson plume shape to distribute ash particles at elevations comparable to the “true” ash  
383 distribution. Even for the best matched results, the high concentration area does not match with observation  
384 well.

385 It is clear that the initial condition of vertical ash distribution has a dominant effect on VATD simulation,  
386 so it is critical for the forecast capability of VATD simulations to explore more accurate and adaptive ways  
387 for establishing the initial ash distribution, especially methods that do not rely on *a posteriori* parameter  
388 calibration or inversion.

### 389 3.2 Effect of Vertical Spread ( $H_{width}$ )

390 In the previous section, we explored the effects of adjusting the plume height to change the vertical  
391 ash distribution at the source. In this section, we investigate the importance of another parameter in the  
392 semiempirical Poisson expression (Eq. (13)). We vary the “vertical spread”,  $H_{width}$ , in the range  $\sim 3 - 10$  km.  
393 A set of initial ash clouds with different vertical spreads are shown in Fig. 8. Except for vertical  
394 spread, all other parameters for creating an initial ash cloud are the same as those in Table 2. The vertical  
395 range within which the majority of ash particles are located becomes narrower when a smaller value for the  
396 vertical spread parameter is used. The ash clouds based on different vertical spread parameters are then  
397 used as initial conditions in Puff simulations.

398 The VATD results are shown in Fig. 11. Adjusting the vertical spread changes particle distribution in  
399 the vertical direction, and thus, not surprisingly, affects the VATD simulation results. None of the VATD  
400 simulations based on initial ash clouds with vertical spreads equal to 3 km or 5 km yield better results than  
401 do VATD simulations based on initial conditions created by Plume-SPH (see Fig. 11). But when we take  
402 10 km as the vertical spread, we get a FMS that is very close to Plume-SPH, even though the shape of the  
403 ash cloud footprint and the maximum height of the ash cloud are completely different.

404 The calibration tests on vertical spread, carried out here, are certainly not exhaustive. One could do a more  
405 comprehensive calibration throughout the multi-dimensional parameter space (for Poisson distribution,  
406 the parameter space is two dimensional) and find better results. In addition, with a more complicated

407 semiempirical plume shape expression, one could have more control over plume shape and might be able  
408 to get an initial condition that yields a more accurate ash transport forecast. However, more complicated  
409 and adaptable plume shape expressions imply a higher dimensional parameter space, which requires more  
410 effort in calibration, even though the degrees of freedom to adjust plume shape are still limited. Creating  
411 initial conditions based on 3D plume simulations avoids such parameter calibration.

### 412 3.3 Horizontal Ash Distribution

413 The differences between the semiempirical plume particle distribution and actual (or simulated by the  
414 3D plume model) are not only in the vertical direction. The importance of the horizontal distance of each  
415 initial ash particle from a line extending upward from the volcano is investigated in this section. Puff  
416 uses a uniformly distributed random process to determine ash particle locations in a circle centered on the  
417 volcano site as described in section 2.2. For the output of Plume-SPH, an effective (maximum) radius is  
418 determined according to a given threshold of ash concentration, following Cerminara et al. (2016b). A time  
419 averaged, spatial integration of the dynamic 3D flow field is conducted to remove significant fluctuations  
420 in time and space. Fig. 9 compares the radius of the initial ash clouds created by 3D plume simulations  
421 with that assumed in the semiempirical plume shape expression adopted in Puff. It is impossible for the  
422 simple, assumed plume shapes to capture the complex and more realistic shapes developed by Plume-SPH.  
423 Additional parameterization may generate more reasonable shapes, but these would continue to be *ad hoc*.  
424 none would likely have the potential fidelity of the 3D simulation to reality, and adding a temporally  
425 changing distribution would be difficult.

426 Comparison between cross-sectional views of the initial ash clouds is shown in Fig. 10. The cross-  
427 sectional view of horizontal particle distribution using the semiempirical method (last figure in Fig. 10)  
428 is similar to a cross-sectional view of a simulated 3D plume, in a general sense. However, for simulated  
429 3D plumes, the ash particle distribution in cross section varies with height, which factor would become  
430 increasingly important with increasing wind speed, were wind speed to be included in the estimate of initial  
431 plume shape. It is difficult for the semiempirical expressions to accommodate such a complex distribution.

432 Despite the obvious difficulty of correctly estimating ash distribution near the vent, or for short  
433 propagation times, assigning different values for the horizontal spread has a negligible effect on VATD  
434 simulation results at large time. We investigated horizontal spread values between 50 km and 1600 km to  
435 create initial ash clouds; all of them generated similar results at large propagation times ( $> 1$  day). Figure  
436 11 shows two different simulation results based on initial ash clouds with horizontal spread equal to 50  
437 km and 600 km, respectively. No visible differences are apparent between them. The FMS values, 0.073  
438 and 0.074, respectively, are also very close. This implies that horizontal distribution has a less significant  
439 influence on VATD simulation results than does vertical distribution for long distance or large time. Perhaps  
440 the most important ramification of this result is that it means the time at which the “handshake” is made  
441 between Plume-SPH and the VATD does not affect results significantly for relatively large distances and  
442 times.

## 4 DISCUSSION

### 443 4.1 Sensitivity of Other Input Parameters

444 Besides the initial ash cloud, other parameters for Puff simulations are: horizontal diffusivity, vertical  
445 diffusivity, mean grain size, grain size standard deviation and total number of tracers. We present in this  
446 subsection informal sensitivity studies on these parameters. We also investigate the influence of eruption

duration. The sensitivity analyses will serve as the basis for identifying possible sources of disparities between simulation and observation.

Fero et al. (2008) simulated the volcanic ash transport in the Pinatubo eruption in 1991. He carried out systematic sensitivity analysis with respect to input parameters of Puff and found that all other parameters except for the plume height have negligible effect on long term ash transportation of Pinatubo. Inspired by Fero et al. (2008), we carried out similar informal sensitivity analysis with much fewer sample points in the parameter space and got similar results. Among the parameters explored, the eruption duration and beginning time show the most obvious influence on simulated ash distribution, although the effect is still small. To show the differences in an intuitive way, (a) - (c) in Fig. 12 shows simulated ash distribution corresponding to 4.9 hours duration, 9 hours duration and 11 hours duration, respectively. After 72 hours, relative to the simulation starting time, these three cases generate very similar results with tiny visible differences. Daniele et al. (2009) did sensitivity analysis with respect to the input parameters of Puff on different volcanoes and found that for eruptive eruptions, the most dominant factors are the wind field and plume height, while all other input parameters are relatively less important. The significance of the wind field has been confirmed by other researchers (Stefanescu et al., 2014, e.g.).

We conducted several simulations with eruption duration varying in the range of [5, 11] hours with slightly different starting time of climactic phase. Table 3 lists all these simulations. However, only slight visible differences are observed among the simulated ash transport outputs. We can see that the eruption duration has negligible effects on long-term ash transport.

The new methodology for generating initial ash clouds introduces a new parameter: elevation threshold, which was specified based on averaged vertical velocity and horizontal velocity. We carry out a separate, informal sensitivity analysis on this parameter by varying the elevation threshold from 1.5 km (the height of the vent) to 25 m. The simulated ash distributions show obvious differences, especially when the elevation threshold is either very high or very low. However, varying the elevation threshold in the range of [12, 18] km generates relatively small differences in ash transport simulation results. Figure 12 (d) and (e) compare the simulated ash distributions corresponding to elevation thresholds of 1.5 km and 15 km. Compared with the ash distribution for a threshold of 15 km, an extra long tail appears when using an elevation threshold of 1.5 km. The maximum height of the tail is around 10 km. Adopting lower elevation thresholds adds more tracer particles at lower elevation. As the winds at different elevations are different, the tracers at lower elevations propagate in different directions. The HYSPLIT forward trajectory tracking indicates that the wind between elevations of 10 km and 15 km blew from north-east to south-west, while winds of higher elevation blew from east to west (see Fig. 6).

## 479 4.2 Other Sources of Disparities

The full range of research issues raised by numerical forecasting of volcanic clouds is diverse. We focused on the effect of initial conditions in this paper. During the plume modeling, secondary factors, such as microphysical processes, even though they play lesser roles, likely need to be included to improve accuracy for a particular eruption. Wind fields are not considered in the current version of Plume-SPH, but for weak plumes, wind plays an important enough role that it has to be considered in the plume model. In addition, eruption conditions are subject to change with time, even during the climactic phase of an eruption. For example, ash just west of Pinatubo observed in satellite images does not show up in “Plume-SPH + Puff” simulation results. This disparity is likely due to the fact that Pinatubo continued erupting (with smaller plume height) after the climactic phase, while we only simulate the climactic phase. In the future, time-dependent initial conditions for VATDs can be created from 3D plume simulations based

490 on time-dependent eruption conditions. It is worth mentioning that the eruption conditions at the vent are  
491 usually inferred from observable information based on 1D plume models. Using a 3D plume model will  
492 not reduce uncertainties from the eruption conditions.

493 Assumption made in each VATD model is another source of errors. For example, a recent study by Osman  
494 et al. (2020) demonstrated the great impact of GSD on modelled ash mass loadings using NAME(Jones  
495 et al., 2007) to simulate historical eruptions of various VEIs. Other researchers (Beckett et al., 2015; Scollo  
496 et al., 2008) have proven the significance of GSD using other VATD models. Their conclusion, however, is  
497 different from our informal sensitivity study and other more comprehensive sensitivity studies using Puff.  
498 This might be because of different assumptions made in different VATD models. These assumptions may  
499 lead to underestimation or overestimation of certain factors, such as GSD. For example, at 55 hours after  
500 eruption, we see an obvious FMS decrease of “Plume-SPH + Puff” results (see (f) in Fig. 5). One of the  
501 important factors that contribute to the big decrease is the fact that these low elevation ash clouds (the west  
502 south portion with small maximum heights) in simulation results are not observed by satellites. This is  
503 probably because Puff underestimates the fallout of ash particles. That is to say, these low elevation ash  
504 clouds should have already fallen onto the ground after 55 hours, but Puff failed to predict their fall onto  
505 ground. This explains why in the sensitivity studies using Puff, the GSD is always not impactful while  
506 sensitivity analysis using other VATD models showing GSD is a significant factor.

507 One implicit assumption in the current method is that ash transportation is dominated by wind advection  
508 (the passive dispersion approximation). However, during the growth of volcanic umbrella, the dominant  
509 factors are various in different regimes (Pouget et al., 2016a) depending on characteristics of a particular  
510 eruption. Webster et al. (2020) suggested that the lateral spread by the intrusive gravity current dominates  
511 the transport of the ash cloud in this stage. Studies by Mastin (Mastin et al., 2014; Mastin and Van Eaton,  
512 2020) also showed that neglecting the umbrella cloud formation for larger eruptions led to significantly  
513 different footprints for the resulting VATD fallout maps. Their studies imply that including mapped  
514 velocities of the plume as a perturbation on the winds can better capture the radial spreading of umbrella.  
515 In the current method, the 3D plume model generated initial ash cloud has a radius around 25 km. For the  
516 Pinatubo 1991 eruption, the passive dispersion approximation can be reasonably applied when radius is  
517 greater than 450 km, and can be fully valid only when the radius is greater than 1800 km (Costa et al., 2013).  
518 So the umbrella stage during the ash transportation is very likely oversimplified in current simulation. It is  
519 computationally too expensive for the Plume-SPH model to continue simulation until the plume radius  
520 reaches, at least, for example, 450 km. An additional umbrella model, with much coarse resolution and  
521 simplified physics, in between the plume model and the VATD model would presumably better model the  
522 whole ash transportation process.

523 Besides the errors from assumptions in the model, errors are also introduced from the reanalysis wind  
524 field data and the satellite observations, which are retrievals, with their associated errors, rather than the  
525 “truth.” In addition, metrics based on footprint can not account for the disparities at different height and ash  
526 concentration. Comparing the simulation and observation purely based on footprint based metric sometimes  
527 is biased.

### 528 4.3 Summary

529 This paper presents, for the first time, VATD simulations using initial source conditions created by a 3D  
530 plume model. Traditional VATD simulations use initial conditions created according to a semiempirical  
531 plume shape expression. A case study of the 1991 Pinatubo eruption demonstrates that a 3D plume model  
532 can create more realistic initial ash cloud and ash parcel positions, and therefore improve the accuracy of

533 ash transport forecasts. Informal sensitivity analyses suggest that initial conditions, as expressed in the  
534 disposition of initial ash parcel positions in the vertical, have a more significant effect on a volcanic ash  
535 transport forecast than most other parameters. Comparison of initial ash parcel distributions among the  
536 3D plume model, semiempirical expressions, and observations suggests that a major subpopulation of ash  
537 parcels should be placed at a much lower elevation than plume height to obtain a better VATD forecast.  
538 Comparing the effects of the plume height, vertical spread and horizontal spread shows that ash particle  
539 distribution in the vertical direction has the strongest effect on VATD simulation results.

540 To summarize, we have presented a novel method for creating *a priori* initial source conditions for  
541 VATD simulations. We have shown that it might be possible to obtain initial positions of ash parcels  
542 with deterministic forward modeling of the volcanic plume, potentially obviating or lessening the need to  
543 attempt to somehow observe initial positions, or *a posteriori* create a history of release heights via inversion  
544 (Stohl et al., 2011). Although the method now suffers from the high computational cost associated with  
545 3D forward modeling, there is the possibility that in future it might not only help overcome shortcomings  
546 of existing methods used to generate *a priori* input parameters, but also overcome the need to carry out  
547 thousands of runs associated with inverse modeling. In addition, computational cost will continue to  
548 diminish as computing speed increases. As they are forward numerical models based on first principles,  
549 3D plume models need little if any parameterization, and user intervention should not be required to  
550 improve forecast power; no assumption about the initial position of ash parcels is needed. Generation of the  
551 initial cloud of ash parcels directly by 3D simulation is potentially adaptable to a variety of volcanic and  
552 atmospheric scenarios. In contrast, semiempirical expressions used to determine initial conditions require  
553 several parameters to control ash particle distribution along a vertical line source or some simplified shape  
554 of the initial ash cloud, making it difficult in some cases to generate initial conditions that closely resemble  
555 a complex reality.

556 The plume-VATD coupling presented in this paper is Lagrangian-Lagrangian coupling. When coupling  
557 plume models and VATD models of different types, the interpolation will be different. For example, to  
558 couple a Lagarian plume model with an Eulerian VATD model, we must convert the particle distribution in  
559 the output of the plume model into ash concentration of cells (mesh grids). When coupling an Eulerian  
560 plume model to a Lagrangian VATD model, the mass fraction of the erupted material in the output of the  
561 3D plume model should be converted into an ash cloud represented by a group of particles. The steps for  
562 coupling a 3D plume model with a VATD model also depends on features of the software, such as the  
563 inputs, the outputs, and file formats.

## CONFLICT OF INTEREST STATEMENT

564 The authors declare that the research was conducted in the absence of any commercial or financial  
565 relationships that could be construed as a potential conflict of interest.

## AUTHOR CONTRIBUTIONS

566 The idea of using a 3D plume model to start a VATD simulation originated from a conservation between  
567 AP and MB. ZC carried out the Plume-SPH simulations, Puff simulations, initial results analysis, and  
568 prepared the first draft. All authors worked together for further revisions. MB carried out the HYSPLIT  
569 simulation. QY post-processed the Puff simulation results, overlapped the simulation results with satellite  
570 observation, and calculated the FMS values. All authors contributed equally to the manuscript writing. AP  
571 and MB obtained funding to financially support the work.

## FUNDING

572 This work was supported by National Science Foundation awards 1521855, 1621853, and 1821311,  
573 1821338 and 2004302 and by the National Research Foundation Singapore and the Singapore Ministry  
574 of Education under the Research Centres of Excellence initiative (project number: NRF2018NRF-  
575 NSFC003ES-010).

## ACKNOWLEDGMENTS

576 We are grateful to the two anonymous reviewers of the paper for their constructive comments and  
577 suggestions that improved the paper. Support for the Twentieth Century Reanalysis Project dataset is  
578 provided by the U.S. Department of Energy, Office of Science Innovative and Novel Computational Impact  
579 on Theory and Experiment (DOE INCITE) program, and Office of Biological and Environmental Research  
580 (BER), and by the National Oceanic and Atmospheric Administration Climate Program Office.

## REFERENCES

- 581 Avdyushin, S., Tulinov, G., Ivanov, M., Kuzmenko, B., Mezhuev, I., Nardi, B., et al. (1993). 1. spatial and  
582 temporal evolution of the optical thickness of the pinatubo aerosol cloud in the northern hemisphere  
583 from a network of ship-borne and stationary lidars. *Geophysical research letters* 20, 1963–1966
- 584 Beckett, F., Witham, C., Hort, M., Stevenson, J., Bonadonna, C., and Millington, S. (2015). Sensitivity of  
585 dispersion model forecasts of volcanic ash clouds to the physical characteristics of the particles. *Journal  
586 of Geophysical Research: Atmospheres* 120, 11–636
- 587 Bonadonna, C., Connor, C. B., Houghton, B., Connor, L., Byrne, M., Laing, A., et al. (2005). Probabilistic  
588 modeling of tephra dispersal: Hazard assessment of a multiphase rhyolitic eruption at tarawera, new  
589 zealand. *Journal of Geophysical Research: Solid Earth* 110
- 590 Bonadonna, C. and Houghton, B. (2005). Total grain-size distribution and volume of tephra-fall deposits.  
591 *Bulletin of Volcanology* 67, 441–456
- 592 Bursik, M. (2001). Effect of wind on the rise height of volcanic plumes. *Geophys. Res. Lett* 28, 3621–3624
- 593 Bursik, M., Jones, M., Carn, S., Dean, K., Patra, A., Pavolonis, M., et al. (2012). Estimation and  
594 propagation of volcanic source parameter uncertainty in an ash transport and dispersal model: application  
595 to the eyjafjallajokull plume of 14–16 april 2010. *Bulletin of volcanology* 74, 2321–2338
- 596 Bursik, M., Kobs, S., Burns, A., Braitseva, O., Bazanova, L., Melekestsev, I., et al. (2009). Volcanic  
597 plumes and wind: Jetstream interaction examples and implications for air traffic. *Journal of Volcanology  
598 and Geothermal Research* 186, 60–67
- 599 Cao, Z., Patra, A., Bursik, M., Pitman, E. B., and Jones, M. (2018). Plume-sph 1.0: a three-dimensional,  
600 dusty-gas volcanic plume model based on smoothed particle hydrodynamics. *Geoscientific Model  
601 Development* 11, 2691–2715
- 602 Cao, Z., Patra, A., and Jones, M. (2017). Data management and volcano plume simulation with parallel  
603 sph method and dynamic halo domains. *Procedia Computer Science* 108, 786–795
- 604 Cerminara, M., Esposti Ongaro, T., and Berselli, L. (2016a). Ashee-1.0: a compressible, equilibrium-  
605 eulerian model for volcanic ash plumes. *Geoscientific Model Development* 9, 697–730
- 606 Cerminara, M., Esposti Ongaro, T., and Neri, A. (2016b). Large eddy simulation of gas–particle kinematic  
607 decoupling and turbulent entrainment in volcanic plumes. *Journal of Volcanology and Geothermal  
608 Research*

- 609 Constantinescu, R., Hopulele-Gligor, A., Connor, C. B., Bonadonna, C., Connor, L. J., Lindsay, J. M.,  
610 et al. (2021). The radius of the umbrella cloud helps characterize large explosive volcanic eruptions.  
611 *Communications Earth & Environment* 2, 1–8
- 612 Costa, A., Folch, A., and Macedonio, G. (2013). Density-driven transport in the umbrella region of volcanic  
613 clouds: Implications for tephra dispersion models. *Geophysical Research Letters* 40, 4823–4827
- 614 Costa, A., Suzuki, Y., Cerminara, M., Devenish, B., Esposti Ongaro, T., Herzog, M., et al. (2016). Results  
615 of the eruptive column model inter-comparison study. *Journal of Volcanology and Geothermal Research*
- 616 Daniele, P., Lirer, L., Petrosino, P., Spinelli, N., and Peterson, R. (2009). Applications of the puff model to  
617 forecasts of volcanic clouds dispersal from etna and vesuvio. *Computers & Geosciences* 35, 1035–1049
- 618 DeFoor, T. E., Robinson, E., and Ryan, S. (1992). Early lidar observations of the june 1991 pinatubo  
619 eruption plume at mauna loa observatory, hawaii. *Geophysical research letters* 19, 187–190
- 620 de'Michieli Vitturi, M., Neri, A., and Barsotti, S. (2015). Plume-mom 1.0: A new integral model of  
621 volcanic plumes based on the method of moments. *Geoscientific Model Development* 8, 2447–2463
- 622 Deshler, T., Hofmann, D., Johnson, B., and Rozier, W. (1992). Balloonborne measurements of the pinatubo  
623 aerosol size distribution and volatility at laramie, wyoming during the summer of 1991. *Geophysical  
624 research letters* 19, 199–202
- 625 Draxler, R. R. and Hess, G. (1998). An overview of the hysplit\_4 modelling system for trajectories.  
626 *Australian meteorological magazine* 47, 295–308
- 627 D'amours, R. (1998). Modeling the etex plume dispersion with the canadian emergency response model.  
628 *Atmospheric Environment* 32, 4335–4341
- 629 Fero, J., Carey, S. N., and Merrill, J. T. (2008). Simulation of the 1980 eruption of mount st. helens using  
630 the ash-tracking model puff. *Journal of Volcanology and Geothermal Research* 175, 355–366
- 631 Fero, J., Carey, S. N., and Merrill, J. T. (2009). Simulating the dispersal of tephra from the 1991  
632 pinatubo eruption: implications for the formation of widespread ash layers. *Journal of Volcanology and  
633 Geothermal Research* 186, 120–131
- 634 Folch, A., Costa, A., and Macedonio, G. (2009). Fall3d: A computational model for transport and  
635 deposition of volcanic ash. *Computers & Geosciences* 35, 1334–1342
- 636 Folch, A., Costa, A., and Macedonio, G. (2016). Fplume-1.0: An integral volcanic plume model accounting  
637 for ash aggregation. *Geoscientific Model Development* 9, 431
- 638 Gingold, R. A. and Monaghan, J. J. (1977). Smoothed particle hydrodynamics: theory and application to  
639 non-spherical stars. *Monthly notices of the royal astronomical society* 181, 375–389
- 640 Guo, S., Bluth, G. J., Rose, W. I., Watson, I. M., and Prata, A. (2004a). Re-evaluation of so2 release  
641 of the 15 june 1991 pinatubo eruption using ultraviolet and infrared satellite sensors. *Geochemistry,  
642 Geophysics, Geosystems* 5
- 643 Guo, S., Rose, W. I., Bluth, G. J., and Watson, I. M. (2004b). Particles in the great pinatubo volcanic cloud  
644 of june 1991: The role of ice. *Geochemistry, Geophysics, Geosystems* 5
- 645 Heffter, J. L. and Stunder, B. J. (1993). Volcanic ash forecast transport and dispersion (vaftad) model.  
646 *Weather and forecasting* 8, 533–541
- 647 Holasek, R., Self, S., and Woods, A. (1996a). Satellite observations and interpretation of the 1991 mount  
648 pinatubo eruption plumes. *Journal of Geophysical Research: Solid Earth* 101, 27635–27655
- 649 Holasek, R. E., Woods, A. W., and Self, S. (1996b). Experiments on gas-ash separation processes in  
650 volcanic umbrella plumes. *Journal of volcanology and geothermal research* 70, 169–181
- 651 Jäger, H. (1992). The pinatubo eruption cloud observed by lidar at garmisch-partenkirchen. *Geophysical  
652 research letters* 19, 191–194

- 653 Jones, A., Thomson, D., Hort, M., and Devenish, B. (2007). The uk met office's next-generation  
654 atmospheric dispersion model, name iii. In *Air pollution modeling and its application XVII* (Springer).  
655 580–589
- 656 Mastin, L. G. (2007). A user-friendly one-dimensional model for wet volcanic plumes. *Geochemistry,*  
657 *Geophysics, Geosystems* 8
- 658 Mastin, L. G. and Van Eaton, A. R. (2020). Comparing simulations of umbrella-cloud growth and ash  
659 transport with observations from pinatubo, kelud, and calbuco volcanoes. *Atmosphere* 11, 1038
- 660 Mastin, L. G., Van Eaton, A. R., and Lowenstern, J. B. (2014). Modeling ash fall distribution from a  
661 yellowstone supereruption. *Geochemistry, Geophysics, Geosystems* 15, 3459–3475
- 662 Neri, A., Esposti Ongaro, T., Macedonio, G., and Gidaspow, D. (2003). Multiparticle simulation of  
663 collapsing volcanic columns and pyroclastic flow. *Journal of Geophysical Research: Solid Earth*  
664 (1978–2012) 108
- 665 Oberhuber, J. M., Herzog, M., Graf, H.-F., and Schwanke, K. (1998). Volcanic plume simulation on large  
666 scales. *Journal of Volcanology and Geothermal Research* 87, 29–53
- 667 Osman, S., Beckett, F., Rust, A., and Snee, E. (2020). Sensitivity of volcanic ash dispersion modelling to  
668 input grain size distribution based on hydromagmatic and magmatic deposits. *Atmosphere* 11, 567
- 669 Paladio-Melosantos, M. L. O., Solidum, R. U., Scott, W. E., Quiambao, R. B., Umbal, J. V., Rodolfo, K. S.,  
670 et al. (1996). Tephra falls of the 1991 eruptions of mount pinatubo. *Fire and mud* 12000, 12030
- 671 Pfeiffer, T., Costa, A., and Macedonio, G. (2005). A model for the numerical simulation of tephra fall  
672 deposits. *Journal of Volcanology and Geothermal Research* 140, 273–294
- 673 Pouget, S., Bursik, M., Johnson, C. G., Hogg, A. J., Phillips, J. C., and Sparks, R. S. J. (2016a).  
674 Interpretation of umbrella cloud growth and morphology: implications for flow regimes of short-lived  
675 and long-lived eruptions. *Bulletin of Volcanology* 78, 1–19
- 676 Pouget, S., Bursik, M., Singla, P., and Singh, T. (2016b). Sensitivity analysis of a one-dimensional model  
677 of a volcanic plume with particle fallout and collapse behavior. *Journal of Volcanology and Geothermal*  
678 *Research*
- 679 Rolph, G., Stein, A., and Stunder, B. (2017). Real-time environmental applications and display system:  
680 Ready. *Environmental Modelling & Software* 95, 210–228
- 681 Schwaiger, H. F., Denlinger, R. P., and Mastin, L. G. (2012). Ash3d: A finite-volume, conservative  
682 numerical model for ash transport and tephra deposition. *Journal of Geophysical Research: Solid Earth*  
683 117
- 684 Scollo, S., Folch, A., and Costa, A. (2008). A parametric and comparative study of different tephra fallout  
685 models. *Journal of Volcanology and Geothermal Research* 176, 199–211
- 686 Scott, W. E., Hoblitt, R. P., Torres, R. C., Self, S., Martinez, M. M. L., and Nillos, T. (1996). Pyroclastic  
687 flows of the june 15, 1991, climactic eruption of mount pinatubo. *Fire and Mud: eruptions and lahars of*  
688 *Mount Pinatubo, Philippines*, 545–570
- 689 Searcy, C., Dean, K., and Stringer, W. (1998). Puff: A volcanic ash tracking and prediction model. *Journal*  
690 *of Volcanology and Geothermal Research* 80, 1–16
- 691 Self, S., Zhao, J.-X., Holasek, R. E., Torres, R. C., and King, A. J. (1996). The atmospheric impact of the  
692 1991 mount pinatubo eruption
- 693 Stefanescu, E., Patra, A. K., Bursik, M., Jones, M., Madankan, R., Pitman, E. B., et al. (2014). Fast  
694 construction of surrogates for uq central to dddas—application to volcanic ash transport. *Procedia*  
695 *Computer Science* 29, 1227–1235

- 696 Stein, A., Draxler, R., Rolph, G., Stunder, B., Cohen, M., and Ngan, F. (2015). Noaa's hysplit atmospheric  
697 transport and dispersion modeling system. *Bulletin of the American Meteorological Society* 96, 2059–  
698 2077
- 699 Stohl, A., Prata, A., Eckhardt, S., Clarisse, L., Durant, A., Henne, S., et al. (2011). Determination of  
700 time-and height-resolved volcanic ash emissions and their use for quantitative ash dispersion modeling:  
701 the 2010 eyjafjallajökull eruption. *Atmospheric Chemistry and Physics* 11, 4333–4351
- 702 Suzuki, T. et al. (1983). A theoretical model for dispersion of tephra. *Arc volcanism: physics and tectonics*  
703 95, 113
- 704 Suzuki, Y. and Koyaguchi, T. (2009). A three-dimensional numerical simulation of spreading umbrella  
705 clouds. *Journal of Geophysical Research: Solid Earth (1978–2012)* 114
- 706 Suzuki, Y. J., Koyaguchi, T., Ogawa, M., and Hachisu, I. (2005). A numerical study of turbulent mixing  
707 in eruption clouds using a three-dimensional fluid dynamics model. *Journal of Geophysical Research: Solid Earth* 110
- 708 Tanaka, H. (1991). Development of a prediction scheme for the volcanic ash fall from redoubt volcano. In  
709 *First Int'l. Symp. on Volcanic Ash and Aviation Safety*. vol. 58
- 710 Tupper, A., Itikarai, I., Richards, M., Prata, F., Carn, S., and Rosenfeld, D. (2007). Facing the challenges of  
711 the international airways volcano watch: the 2004/05 eruptions of manam, papua new guinea. *Weather and Forecasting* 22, 175–191
- 712 Walko, R., Tremback, C., and Bell, M. (1995). Hypact: The hybrid particle and concentration transport  
713 model. *User's guide*
- 714 Webster, H. N., Devenish, B. J., Mastin, L. G., Thomson, D. J., and Van Eaton, A. R. (2020). Operational  
715 modelling of umbrella cloud growth in a lagrangian volcanic ash transport and dispersion model.  
716 *Atmosphere* 11, 200
- 717 Witham, C., Hort, M., Potts, R., Servranckx, R., Husson, P., and Bonnardot, F. (2007). Comparison of  
718 vaac atmospheric dispersion models using the 1 november 2004 grimsvötn eruption. *Meteorological Applications* 14, 27–38
- 719 Woods, A. (1988). The fluid dynamics and thermodynamics of eruption columns. *Bulletin of Volcanology*  
720 50, 169–193
- 721 Zidikheri, M. J., Lucas, C., and Potts, R. J. (2017). Estimation of optimal dispersion model source  
722 parameters using satellite detections of volcanic ash. *Journal of Geophysical Research: Atmospheres*  
723 122, 8207–8232

## FIGURE CAPTIONS

727 T

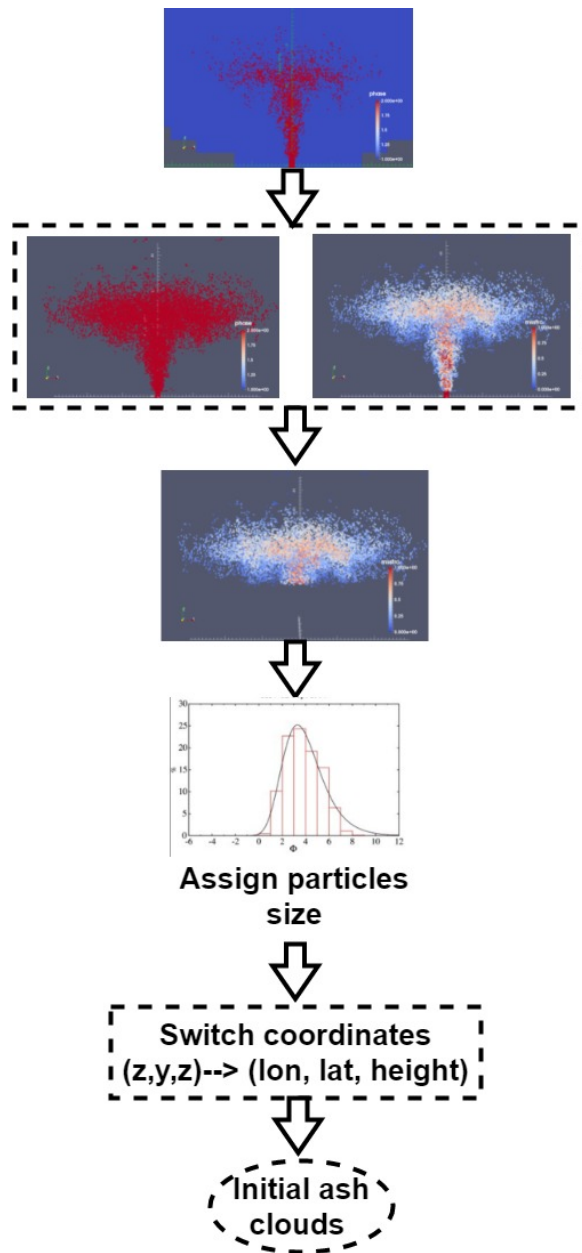


**Figure 1.** Steps to create initial condition for Puff based on raw output of Plume-SPH (Cao et al., 2018). First row: raw output of Plume-SPH. Blue particles are phase 1 (ambient air), red particles are phase 2 (erupted material). Second row: plume after removing SPH particles of phase 1. Picture at right is colored according to the mass fraction of erupted material. Third row: volcanic plume above the “corner” region after cutting off the lower portion. Fourth row: assign sizes to particles converting numerical discretization points into tracers. Fifth row: switch coordinates in local coordinate system into (*longitude*, *latitude*, *height*)

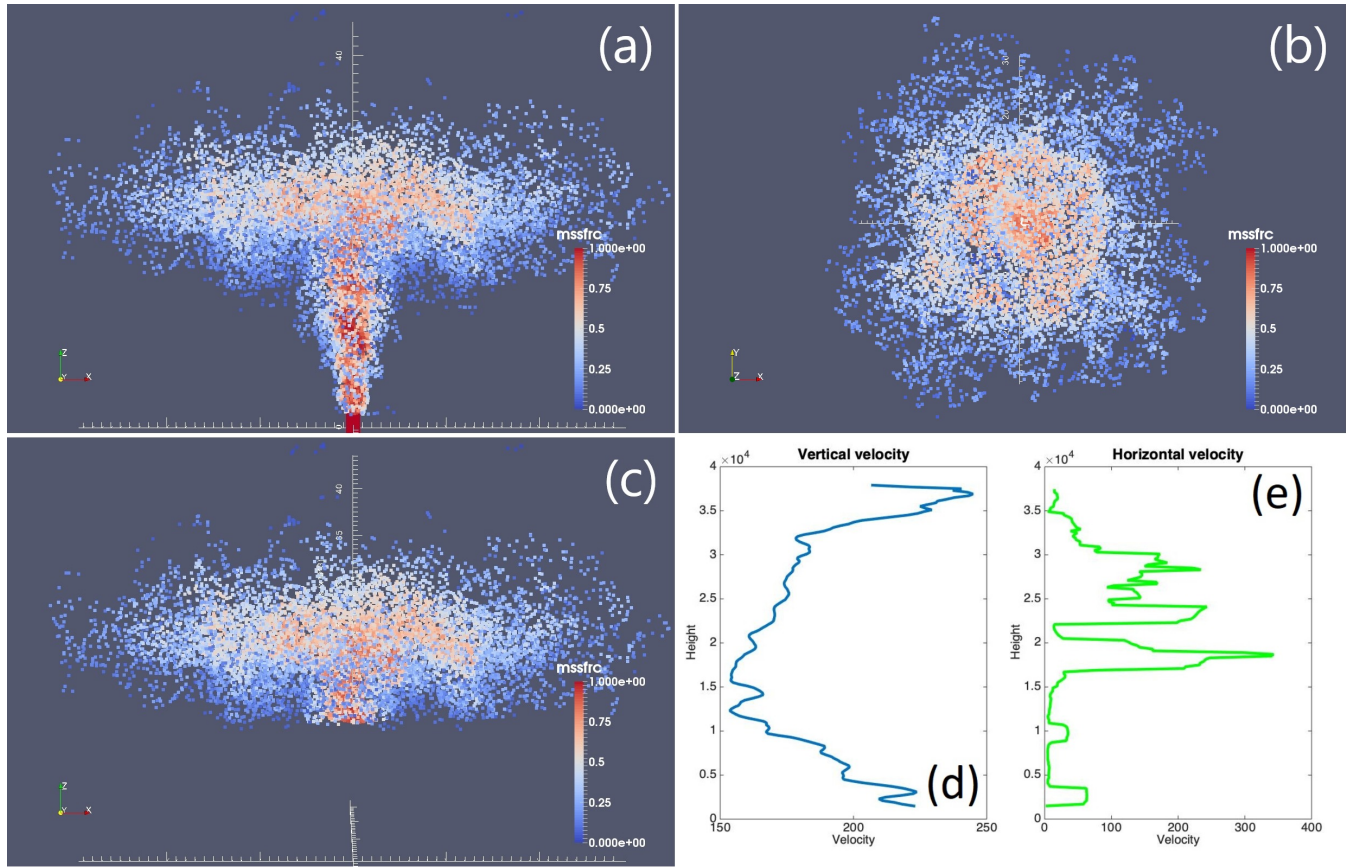


**Figure 2.** Volcano plume from 3D plume model. All particles in the pictures are of phase 2 (particle of phase 1 has been removed) at 600s after eruption, at which time, the plume has already reached the plume height and started spreading radially. (a) is the front view of the whole plume. (b) is the top view of the plume. (c) is the front view of the initial ash cloud, which is essentially a portion of the whole plume whose elevation is higher than a given threshold (in this picture is 15 km). Particles are colored according to mass fraction of erupted material. Red represents high mass fraction while blue represents low mass fraction. (d) is the average vertical velocity of the plume. At elevations below 15 km, the average vertical velocity decreases. At elevations higher than 15 km, the averaged vertical velocity starts increasing. (e) is the average horizontal velocity of the plume. The averaged horizontal velocity becomes obviously larger when elevation is higher than 15 km. So the reflection point is somewhere around 15 km.

**Table 1.** List of eruption condition and material properties for plume simulation

Parameters	Units	Plume
Vent Velocity	$\text{m} \cdot \text{s}^{-1}$	275
Vent Gas Mass Fraction		0.05
Vent Temperature	K	1053
Vent Height	m	1500
Mass Discharge Rate	$\text{kg} \cdot \text{s}^{-1}$	$1.5 \times 10^9$
Specific Heat of Gas at Constant Volume	$\text{J} \cdot \text{kg}^{-1} \cdot \text{K}^{-1}$	717
Specific Heat of Air at Constant Volume	$\text{J} \cdot \text{kg}^{-1} \cdot \text{K}^{-1}$	1340
Specific Heat of Solid	$\text{J} \cdot \text{kg}^{-1} \cdot \text{K}^{-1}$	1100
Specific Heat of Gas at Constant Pressure	$\text{J} \cdot \text{kg}^{-1} \cdot \text{K}^{-1}$	1000
Specific Heat of Air at Constant Pressure	$\text{J} \cdot \text{kg}^{-1} \cdot \text{K}^{-1}$	1810
Density of Air at Vent Height	$\text{kg} \cdot \text{m}^{-3}$	1.104
Pressure at Vent Height	Pa	84363.4

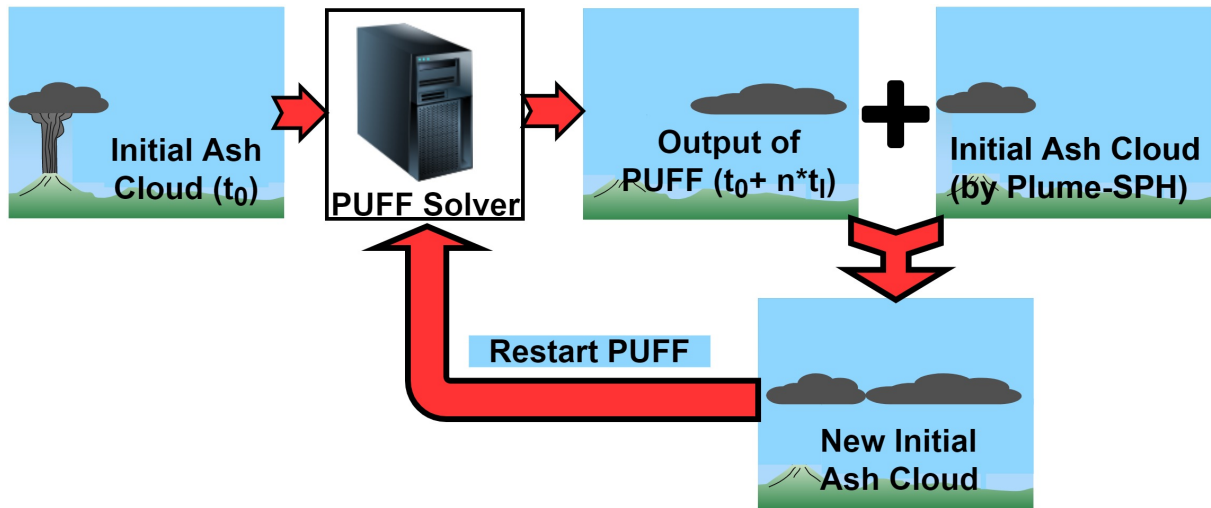


**Figure 3.** Mimic successive eruption with intermittent pulsed releasing of ash particles.  $t_I$  is the period of pulsing release.  $t_I$  equals the physical time of 3D plume simulation.

**Table 2.** Parameters used in VATD simulation of the climactic phase of Pinatubo eruption on June 15 1991. The first six parameters are used by semiempirical expression to create an initial ash cloud. When creating an initial condition based on the Plume-SPH model, these parameters are extracted from output of Plume-SPH model.

Parameters	Unit	Semiempirical	Plume-SPH
Plume Height ( $H_{max}$ )	km	40	-
Horizontal Spread ( $r_{max}$ )	km	103.808	-
Vertical Spread ( $H_{width}$ )	km	6.662	-
Plume Shape	-	Poisson	-
Total Ash Particles	-	1768500	1768500
Elevation Threshold	m	-	15000
Horizontal Diffusivity	$m^2/s$	10000	10000
Vertical Diffusivity	$m^2/s$	10	10
Grain Size Distribution	-	Gaussian	Gaussian
Mean of Grain Size (Radius)	mm	$3.5 \times 10^{-2}$	$3.5 \times 10^{-2}$
Standard Deviation of Grain Size	-	1.0	1.0
Start Time	UT	0441	0441
End time	UT	1341	1341
Simulation Duration	hour	72	72

**Table 3.** The starting and ending time (UT) for simulating the climactic phase of Pinatubo eruption on June 15 1991. Observed plume height (Holasek et al., 1996a) at different time are also listed in the table.

Eruption Duration	4.9 hours	9 hours	10 hours	11.1 hours
Start Time	0441	0441	0441	0334
Height at Start Time	37.5 km	37.5 km	37.5 km	24.5 km
End Time	0934	1341	1441	1441
Height at End Time	35 km	26.5 km	22.5	22.5 km

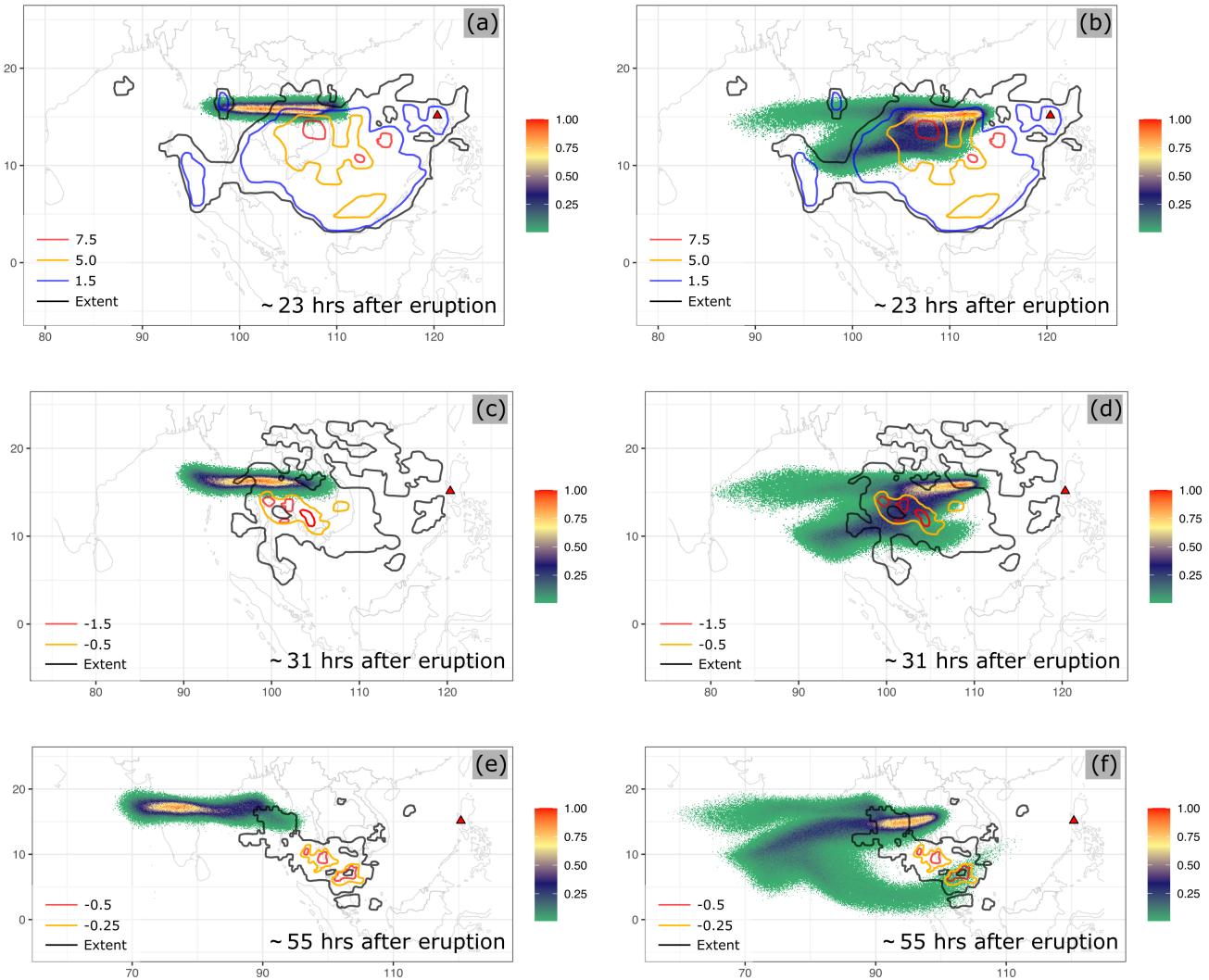


**Figure 4.** Comparison between “Semiempirical initial cloud + Puff” and “Plume-SPH + Puff”. Pictures to the left are: Puff simulation based on initial condition created according to semiempirical plume shape expression. Pictures to the right are Puff simulation based on initial conditions generated by Plume-SPH. TOMS or AVHRR images of Pinatubo ash cloud are overlapped with the simulation results. Ash clouds at different hours after eruption are on different rows. From top to bottom, the images correspond to around 23 hours after eruption (UT 199106160341), 31 hours after eruption (UT 199106161141), 55 hours after eruption (UT 199106171141). The observation data on the first row are TOMS ash and ice map. The observation data on the second and third row are AVHRR BTD ash cloud map with atmospheric correction method applied (Guo et al., 2004b). The contours of simulation results are maximum concentration at given (*longitude, latitude*).

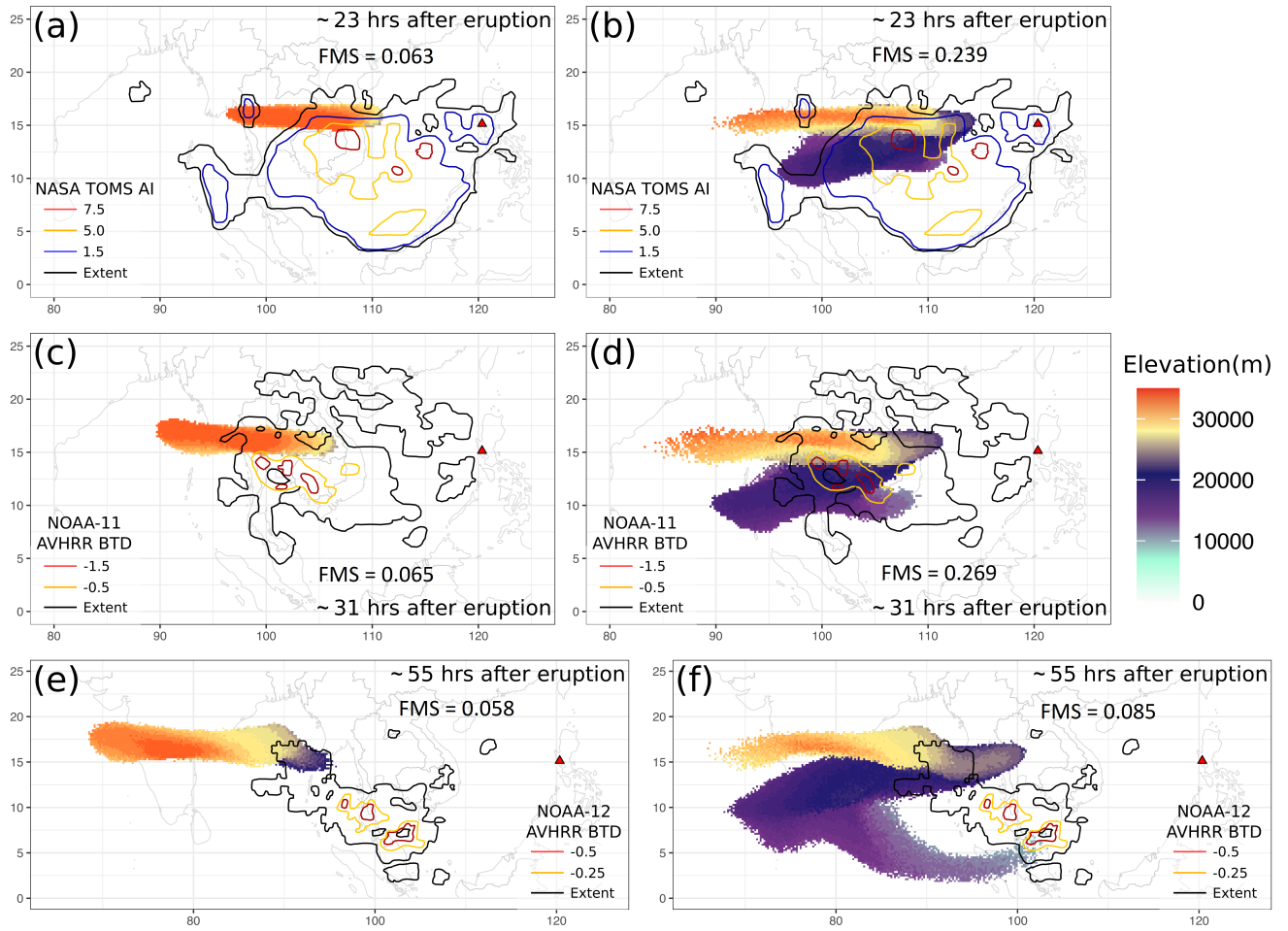


**Figure 5.** Comparison between “Semiempirical initial cloud + Puff” and “Plume-SPH + Puff”. Pictures to the left are: Puff simulation based on initial condition created according to semiempirical plume shape expression. Pictures to the right are Puff simulation based on initial conditions generated by Plume-SPH. TOMS or AVHRR images of Pinatubo ash cloud are overlapped with the simulation results. Ash clouds at different hours after eruption are on different rows. From top to bottom, the images correspond to around 23 hours after eruption (UT 199106160341), 31 hours after eruption (UT 199106161141), 55 hours after eruption (UT 199106171141). The observation data on the first row are TOMS ash and ice map. The observation data on the second and third row are AVHRR BTD ash cloud map with atmospheric correction method applied (Guo et al., 2004b). The contours of simulation results are maximum height of ash cloud. The FMS value for each simulation is on each contour.

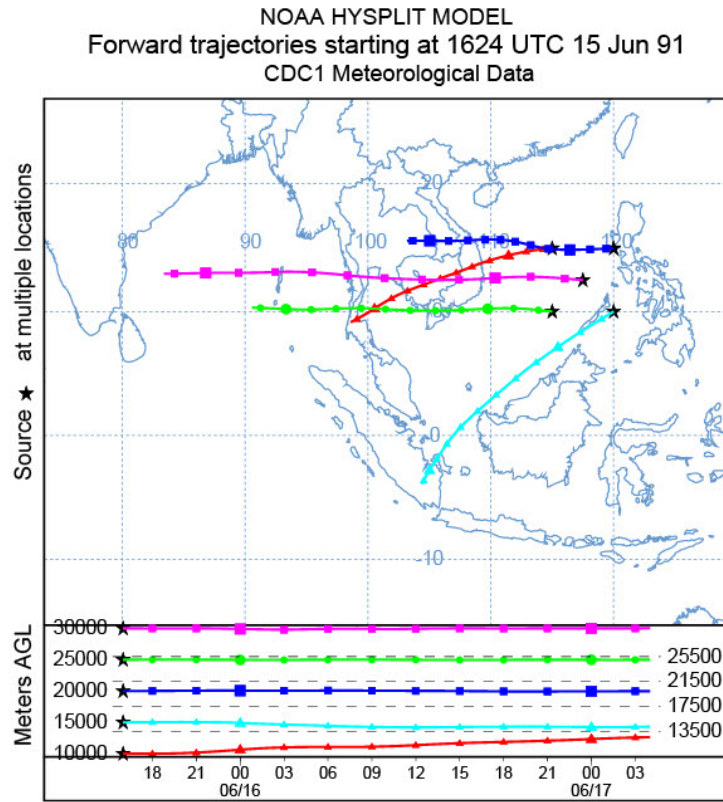


**Figure 6.** Trajectories of particles starting from different heights indicating the wind directions of different evaluations. The trajectories are chosen to start at points that were on the perimeter of the umbrella cloud in  $x$ ,  $y$  and  $z$ , and in its center, right before it became affected by the wind to give an idea of the maximum possible spread of the trajectories from that initial condition.

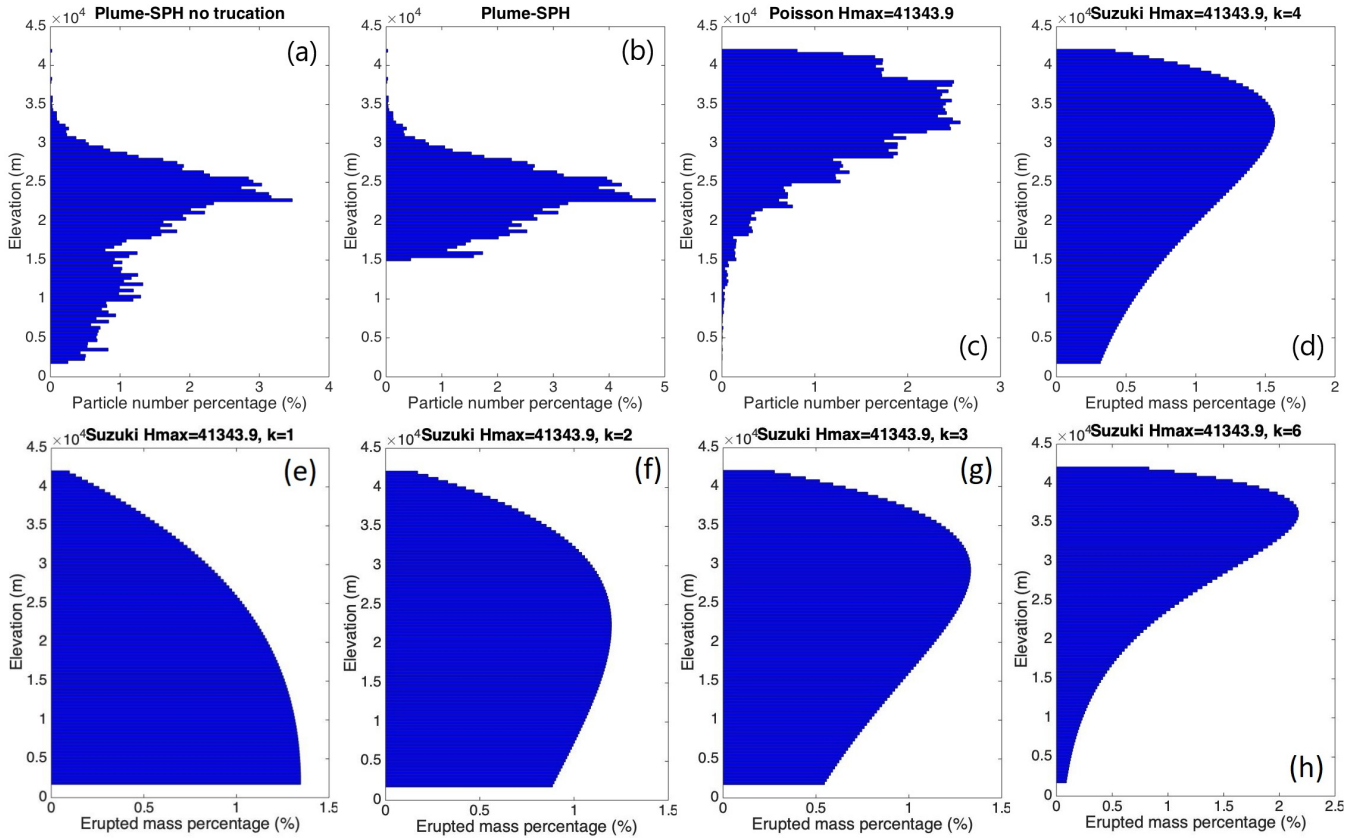


**Figure 7.** First row, comparison of particle distribution of initial ash cloud in vertical direction. (a) is corresponding to the initial ash cloud obtained from Plume-SPH output. (b) is (a) truncated by a elevation threshold of 15 km. (c) is for vertical ash distribution based on Poisson distribution (Eq. (13)) with  $H_{max}$  equals to 40 km. Another parameter,  $H_{width}$  is 6662 m. (d) is corresponding to Suzuki distribution (Eq. (14)) with  $H_{max}$  equals to 40 km and  $k$  equals to 4(Pfeiffer et al., 2005). The second row, Suzuki distribution with  $H_{max}$  equals to 40 km but different values for  $k$ . The  $x$  axis is the percentage of particle numbers for Plume-SPH and Poisson. For Suzuki the  $x$  axis is the mass percentage of erupted material.

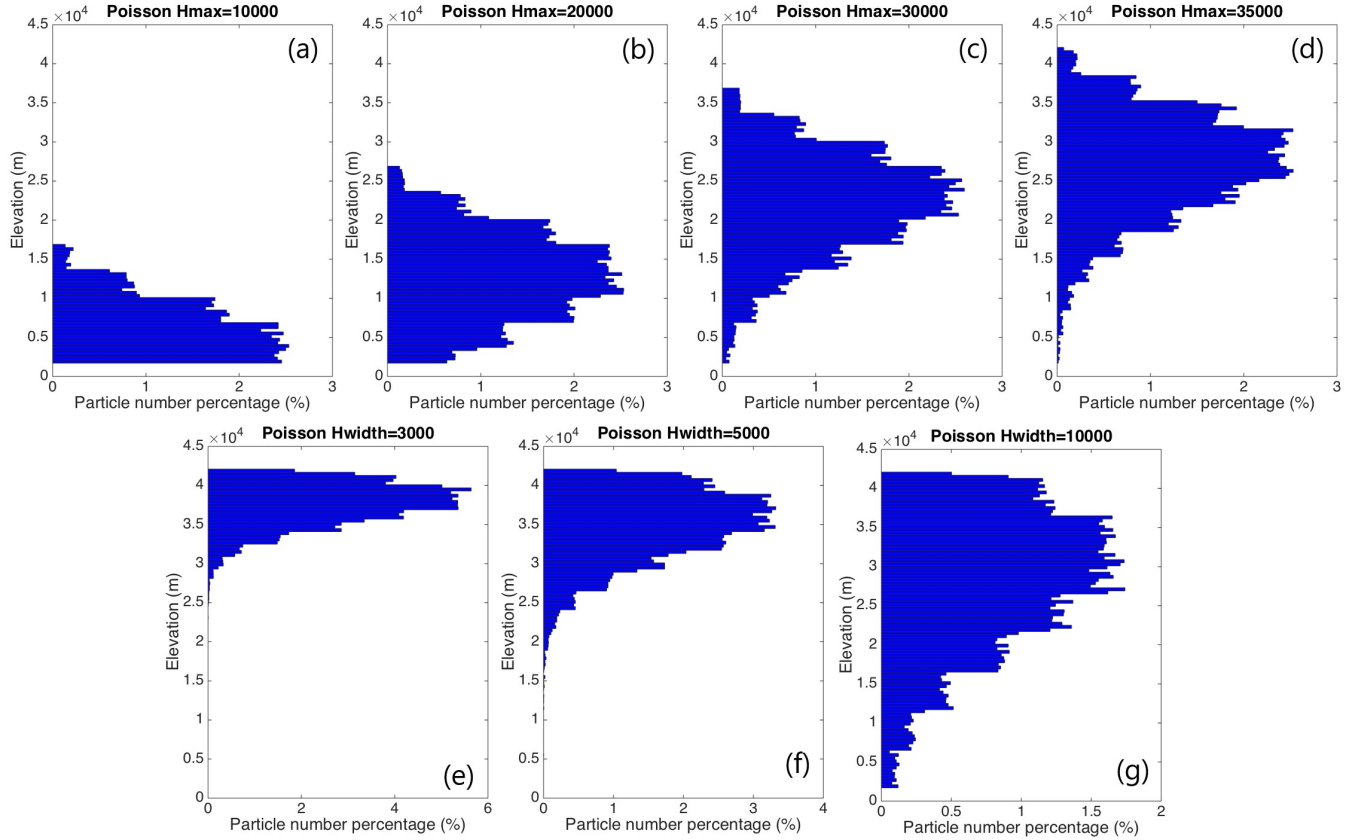


**Figure 8.** Initial particle distribution in vertical direction based on Poisson plume shape (Eq. (13)). The first row varies plume heights. (a) to (d) are corresponding to plume height of 10 km, 20 km, 30 km, 35 km. Another parameter,  $H_{width}$  is 6662 m for all four figures in the first row. The second row varies “vertical spread”,  $H_{width}$ . (e) to (g) are corresponding to vertical spread of 3 km, 5 km and 10 km. The plume height,  $H_{max}$  is set to 40 km for all three figures. The  $x$  axis is the percentage of particle numbers. See Fig. 7 for vertical ash distribution of Plume-SPH output.

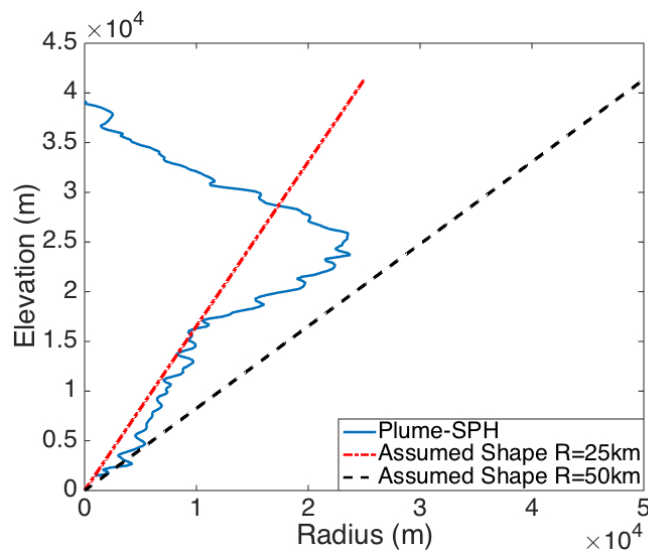


**Figure 9.** Comparison between radius of initial ash clouds created by 3D plume model (Plume-SPH) and assumed initial ash cloud shape (Eq. 15) in Puff. The plume shape expression used in Puff defines an inverted cone whose actual shape changes when “horizontal spread” takes different values.  $R = 25\text{ km}$  is corresponding to “horizontal spread” equals to  $50\text{ km}$ .  $R = 50\text{ km}$  is corresponding to “horizontal spread” equals to  $100\text{ km}$

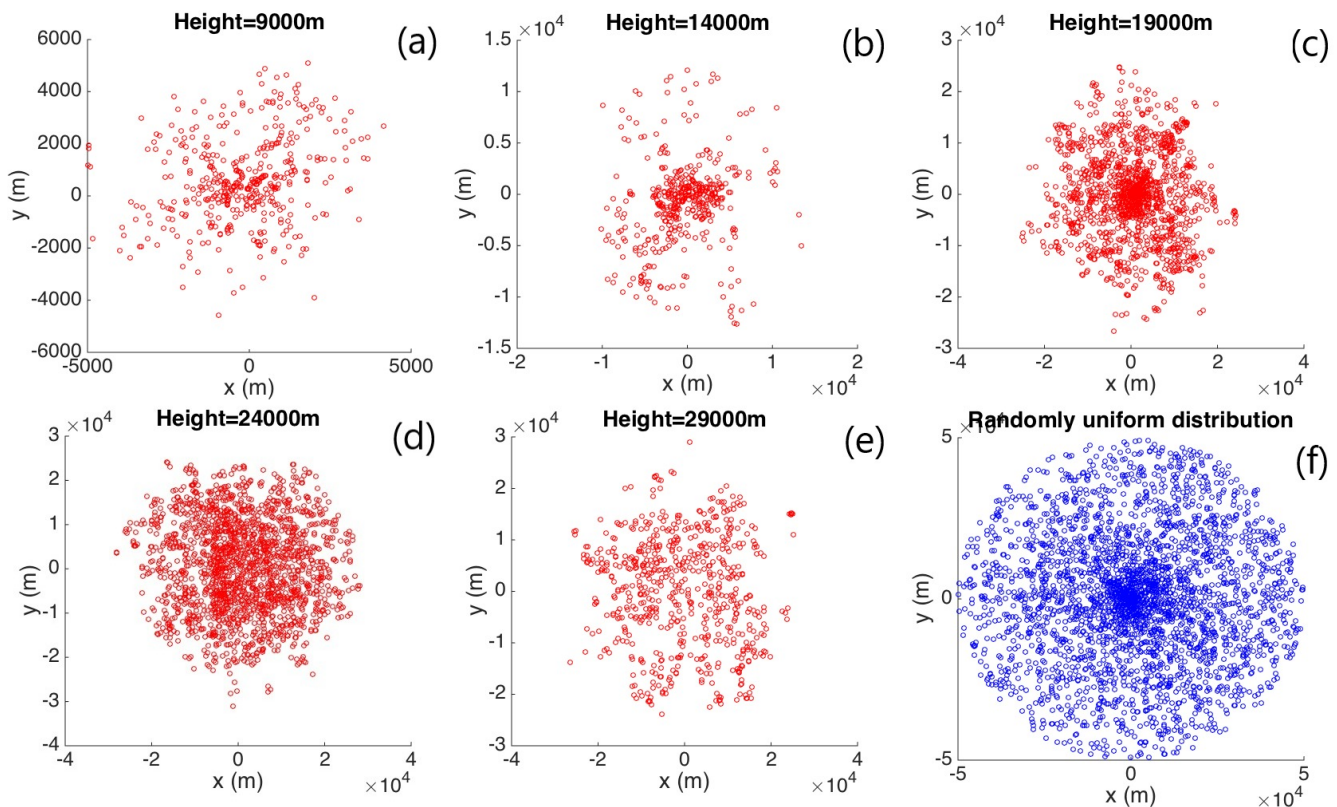


**Figure 10.** Horizontal distribution of ash particles (tracers) on a cross section of initial ash cloud. Puff assumes a randomly uniform distribution of ash particles within a circle, as shown by blue dots in (f). All other figures show the ash particle distribution of initial ash clouds created by Plume-SPH at different elevations.

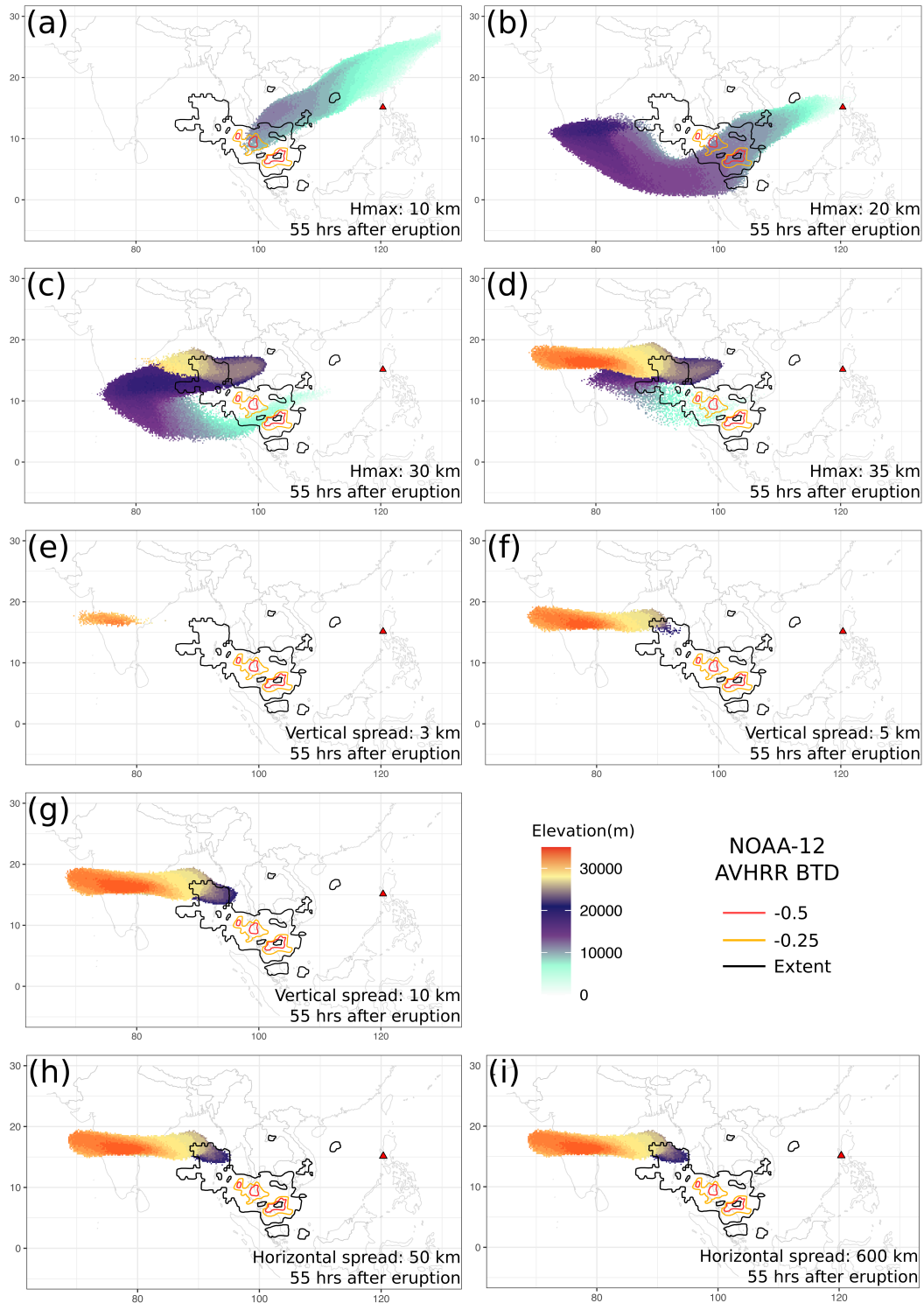


**Figure 11.** Ash transport simulated by Puff using different initial ash clouds created according the empirical expressions using different input parameters. All images are corresponding to 55 hours after eruption (UT 199106171141). More details are in the table below

Parameter	$H_{max}$				$H_{width}$			$r_{max}$	
Value	10 km	20 km	30 km	35 km	3 km	5km	10 km	50 km	600 km
Plot	(a)	(b)	(c)	(d)	(e)	(f)	(g)	(h)	(i)
FMS	0.055	0.121	0.142	0.227	0	0.039	0.085	0.073	0.074

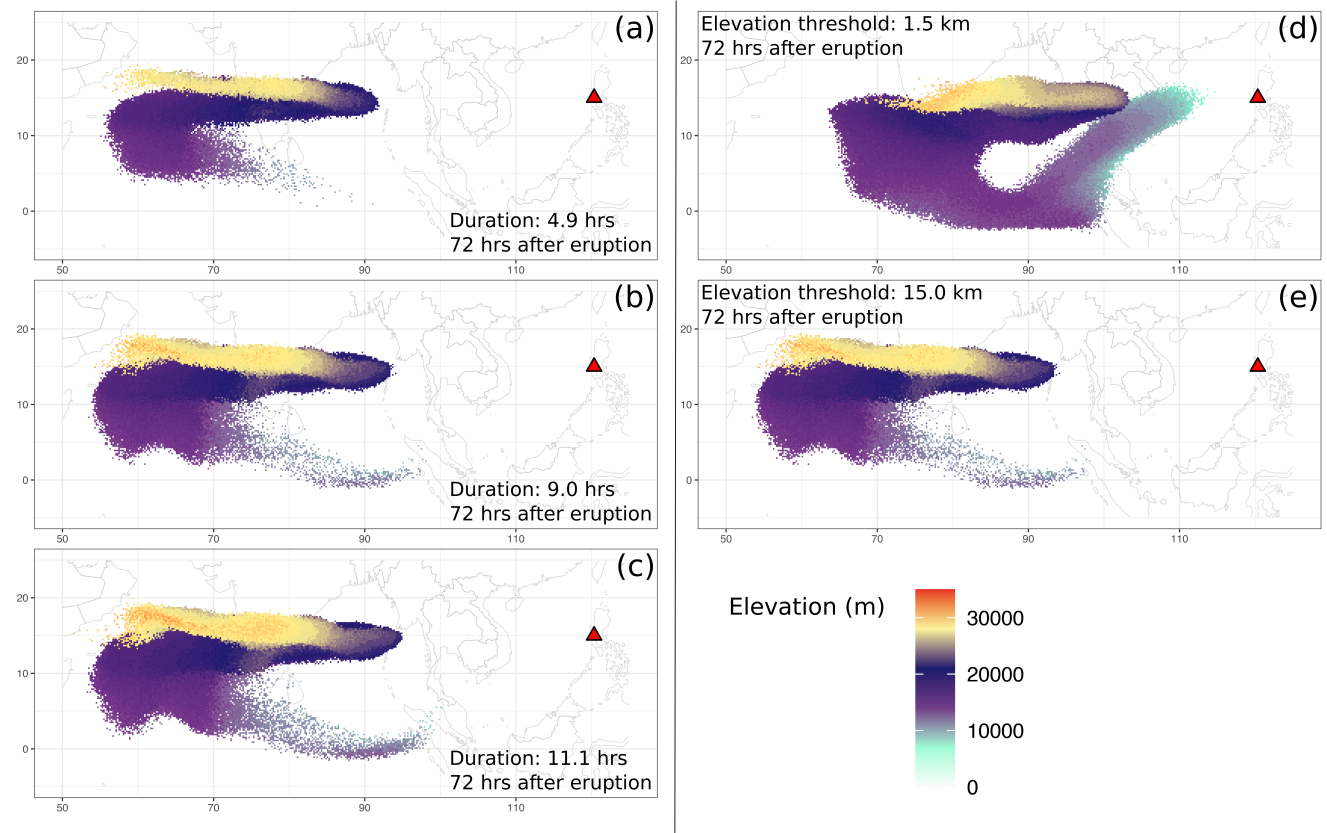


**Figure 12.** Sensitivity of Puff simulation with respect to eruption durations and initial ash cloud cutoff heights (elevation threshold). For different eruption durations, the starting and ending time for each case is in Table 3. The contours correspond to ash concentration at 72 hours after eruption. Details are in the table below.

Parameter	Eruption Duration			Elevation Threshold	
Value	4.9 hour	9 hour	11.1 hour	1500 m	15 km
Plot	(a)	(b)	(c)	(d)	(e)